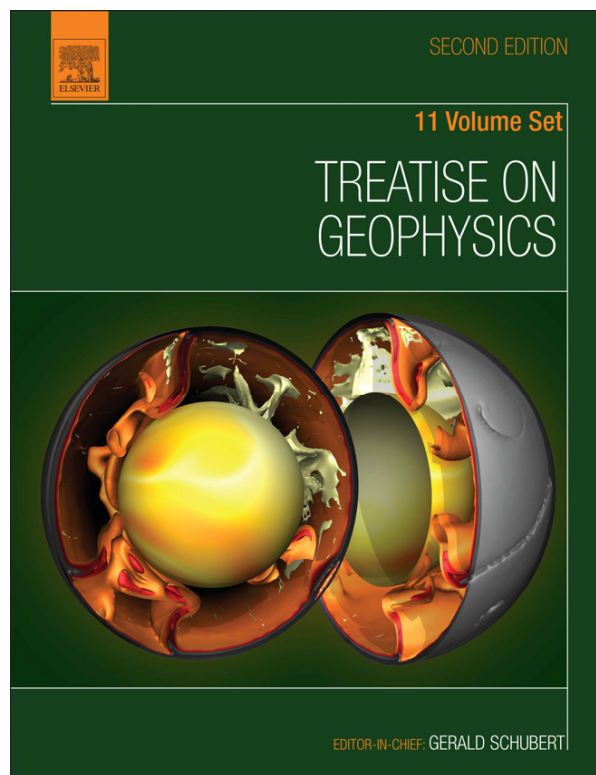


Provided for non-commercial research and educational use.
Not for reproduction, distribution or commercial use.

This article was originally published in *Treatise on Geophysics, Second Edition*, published by Elsevier, and the attached copy is provided by Elsevier for the author's benefit and for the benefit of the author's institution, for non-commercial research and educational use including without limitation use in instruction at your institution, sending it to specific colleagues who you know, and providing a copy to your institution's administrator.



All other uses, reproduction and distribution, including without limitation commercial reprints, selling or licensing copies or access, or posting on open internet sites, your personal or institution's website or repository, are prohibited. For exceptions, permission may be sought for such use through Elsevier's permissions site at:

<http://www.elsevier.com/locate/permissionusematerial>

Blewitt G GPS and Space-Based Geodetic Methods. In: Gerald Schubert (editor-in-chief) *Treatise on Geophysics*, 2nd edition, Vol 3. Oxford: Elsevier; 2015. p. 307-338.

3.11 GPS and Space-Based Geodetic Methods

G Blewitt, University of Nevada, Reno, NV, USA

© 2015 Elsevier B.V. All rights reserved.

3.11.1	The Development of Space Geodetic Methods	307
3.11.1.1	Introduction	307
3.11.1.2	The Limitations of Classical Surveying Methods	308
3.11.1.3	The Impact of Space Geodesy	309
3.11.1.4	Lunar Laser Ranging Development	310
3.11.1.5	Satellite Laser Ranging Development	310
3.11.1.6	VLBI Development	311
3.11.1.7	Global Positioning System Development	311
3.11.1.8	Comparing GPS with VLBI and SLR	313
3.11.1.9	GPS Receivers in Space: LEO GPS	314
3.11.1.10	Global Navigation Satellite Systems	314
3.11.1.11	International GNSS Service	315
3.11.2	GPS and Basic Principles	316
3.11.2.1	Basic Principles	316
3.11.2.2	GPS Design and Consequences	318
3.11.2.3	Introducing High-Precision GPS	319
3.11.2.4	GPS Observable Modeling	321
3.11.2.5	Data Processing Software	324
3.11.2.6	Real-Time GPS and Accuracy Versus Latency	326
3.11.3	Global and Regional Measurement of Geophysical Processes	326
3.11.3.1	Introduction	326
3.11.3.2	Estimation of Station Velocity	328
3.11.3.3	Plate Tectonic Rotations	329
3.11.3.4	Plate Boundary Strain Accumulation	330
3.11.3.5	The Earthquake Cycle	332
3.11.3.6	Surface Mass Loading	334
References		335

3.11.1 The Development of Space Geodetic Methods

3.11.1.1 Introduction

Geodesy is the science of accurately measuring and understanding three fundamental properties of the Earth: (1) its gravitational field, (2) its geometric shape, and (3) its orientation in space (Torge, 2001). In recent decades, the growing emphasis has been on the time variation of these 'three pillars of geodesy' (Beutler et al., 2004), which has become possible owing to the accuracy of new space-based geodetic methods and also owing to a truly global reference system that only space geodesy can realize (Altamimi et al., 2001, 2002). As each of these three properties is connected by physical laws and is forced by natural processes of scientific interest (Lambeck, 1988), thus, space geodesy has become a highly interdisciplinary field, intersecting with a vast array of geophysical disciplines, including tectonics, Earth structure, seismology, oceanography, hydrology, atmospheric physics, meteorology, and climate change. This richness of diversity has provided the impetus to develop space geodesy as a precise geophysical tool that can probe the Earth and its interacting spheres in ways never before possible (Smith and Turcotte, 1993).

Borrowing from the fields of navigation and radio astronomy and classical surveying, space geodetic methods were

introduced in the early 1970s with the development of lunar laser ranging (LLR), satellite laser ranging (SLR), and very long baseline interferometry (VLBI) and soon to be followed by the Global Positioning System (GPS) (Smith and Turcotte, 1993). The near future promises other new space geodetic systems similar to GPS, which can be more generally called Global Navigation Satellite Systems (GNSSs). In recent years, the GPS has become commonplace, serving a diversity of applications from car navigation to surveying. Originally designed for few meter-level positioning for military purposes, GPS is now routinely used in many areas of geophysics (Billham, 1991; Dixon, 1991; Hager et al., 1991; Segall and Davis, 1997), for example, to monitor the movement of the Earth's surface between points on different continents with millimeter-level precision, essentially making it possible to observe plate tectonics as it happens.

The stringent requirements of geophysics are part of the reason as to why GPS has become as precise as it is today (Blewitt, 1993). As will be described here, novel techniques have been developed by researchers working in the field of geophysics and geodesy, resulting in an improvement of GPS precision by four orders of magnitude over the original design specifications. Owing to this high level of precision and the relative ease of acquiring GPS data, GPS has revolutionized geophysics, as well as many other areas of human endeavor (Minster et al., 2010).

Whereas perhaps the general public may be more familiar with the georeferencing applications of GPS, say, to locate a vehicle on a map, this chapter introduces space geodetic methods with a special focus on GPS as a high-precision geodetic technique and introduces the basic principles of geophysical research applications that this capability enables. As an example of the exacting nature of modern GPS geodesy, [Figure 1](#) shows a geodetic GPS station of commonplace (but leading-edge) design now in the western United States, installed for purposes of measuring tectonic deformation across the boundary between the North American and Pacific plates. This station was installed in 1996 at Slide Mountain, Nevada, as part of the BARGEN network ([Bennett et al., 1998, 2003](#); [Wernicke et al., 2000](#)). To mitigate the problem of very local, shallow surface motions ([Wyatt, 1982](#)), this station has a deep brace Wyatt-type monument design, by which the antenna is held fixed to the Earth's crust by four welded braces that are anchored ~ 10 m below the surface (and are decoupled by padded boreholes from the surface). Tests have shown that such monuments exhibit less environmentally caused displacement than those installed to a (previously more common) depth of ~ 2 m ([Langbein et al., 1995](#)). Time series of daily coordinate estimates from such sites indicate repeatability at the level of 1 mm horizontal, and 3 mm vertical, with a velocity uncertainty of 0.2 mm year^{-1} ([Davis et al., 2003](#)). This particular site detected ~ 10 mm of transient motion for 5 months in late 2003, concurrent with unusually deep seismicity below Lake Tahoe that was likely caused by intrusion of magma into the lower crust ([Smith et al., 2004](#)).

3.11.1.2 The Limitations of Classical Surveying Methods

It is useful to consider the historical context of terrestrial surveying at the dawn of modern space geodesy around 1970 ([Bomford, 1971](#)). Classical geodetic work of the highest (\sim mm) precision was demonstrated in the 1970s for purposes of measuring horizontal crustal strain over regional scales (e.g., [Savage, 1983](#)). However, the limitations of classical geodesy discussed in the succeeding text implied that it was essentially impossible to advance geodetic research on the global scale.



Figure 1 Permanent IGS station at Slide Mountain, Nevada, the United States. Photo by Jean Dixon.

Classical surveying methods were not truly three-dimensional. This is because geodetic networks were distinctly separated into horizontal networks and height networks, with poor connections between them. Horizontal networks relied on the measurement of angles (triangulation) and distances (trilateration) between physical points (or 'benchmarks') marked on top of triangulation pillars, and vertical networks mainly depended on spirit leveling between height benchmarks. In principle, height networks could be loosely tied to horizontal networks by collocation of measurement techniques at a subset of benchmarks, together with geometric observations of vertical angles. Practically, this was difficult to achieve, because of the differing requirements on the respective networks. Horizontal benchmarks could be separated further apart on hill tops and peaks, but height benchmarks were more efficiently surveyed along valleys wherever possible. Moreover, the measurement of angles is not particularly precise and is subject to significant systematic error, such as atmospheric refraction.

Fundamentally, however, the height measured with respect to the gravitational field (by spirit leveling) is not the same quantity as the geometric height, which is given relative to some conventional ellipsoid (that in some average sense represents sea level). Thus, the horizontal and height coordinate systems (often called a '2+1' system) could never be made entirely consistent.

A troublesome aspect of terrestrial surveying methods was that observations were necessarily made between benchmarks that were relatively close to each other, typically between nearest neighbors in a network. Because of this, terrestrial methods suffered from increase in errors as the distance increased across a network. Random errors would add together across a network, growing as a random walk process, proportional to the square root of distance.

Even worse, systematic errors in terrestrial methods (such as errors correlated with elevation, temperature, latitude, etc.) can grow approximately linearly with distance. For example, wave propagation for classical surveying occurs entirely within the troposphere, and thus, errors due to refraction increase with the distance between stations. In contrast, no matter how far apart the stations are, wave propagation for space geodetic techniques occurs almost entirely in the approximate vacuum of space and is only subject to refraction within ~ 10 km optical thickness of the troposphere (and within the ionosphere in the case of microwave techniques, although ionospheric refraction can be precisely calibrated by dual-frequency measurements). Furthermore, by modeling the changing slant depth through the troposphere (depending on the source position in the sky), tropospheric delay can be accurately estimated as part of the positioning solution.

There were other significant problems with terrestrial surveying that limited its application to geophysical geodesy. One was the requirement of interstation visibility, not only with respect to intervening terrain but also with respect to the weather at the time of observation. Furthermore, the precision and accuracy of terrestrial surveying depended a lot on the skill and experience of the surveyors making the measurements and the procedures developed to mitigate systematic error while in the field (i.e., errors that could not readily be corrected after the fact).

Finally, the spatial extent of classical terrestrial surveying was limited by the extent of continents. In practice, different

countries often adopted different conventions to define the coordinates of their national networks. As a consequence, each nation typically had a different reference system. More importantly from a scientific viewpoint, connecting continental networks across the ocean was not feasible without the use of satellites. So in the classical geodetic era, it was possible to characterize the approximate shape of the Earth; however, the study of the change of the Earth's shape in time was for all practical purposes out of the question.

3.11.1.3 The Impact of Space Geodesy

Space geodetic techniques have since solved all the aforementioned problems of terrestrial surveying. Therefore, the impact of space geodetic techniques can be summarized as follows (as will be explained in detail later):

- They allow for true three-dimensional positioning.
- They allow for relative positioning that does not degrade significantly with distance.
- They do not require interstation visibility and can tolerate a broader range of weather conditions.
- The precision and accuracy are far superior and position estimates are more reproducible and repeatable than for terrestrial surveying, where for space geodesy, the quality is determined more by the quality of the instruments and data processing software than by the skill of the operator.
- They allow for global networks that can define a global reference frame; thus, the position coordinates of stations in different continents can be expressed in the same system.

From a geophysical point of view, the advantages of space geodetic techniques can be summarized as follows:

- The high precision of space geodesy (now at the ~ 1 mm level), particularly over very long distances, allows for the study of Earth processes that could never be observed with classical techniques.
- The Earth's surface can be surveyed in one consistent reference frame, so geophysical processes can be studied in a consistent way over distance scales ranging ten orders of magnitude from 10^0 to 10^{10} m (Altamimi et al., 2002). Global surveying allows for the determination of the largest-scale processes on Earth, such as plate tectonics and surface mass loading.
- Geophysical processes can be studied in a consistent way over timescales ranging ten orders of magnitude from 10^{-1} to 10^9 s. Space geodetic methods allow for continuous acquisition of data using permanent stations with communications to a data processing center. This allows for geophysical processes to be monitored continuously, which is especially important for the monitoring of natural hazards but is also important for the characterization of errors and for the enhancement of precision in the determination of motion. Sample rates from GPS can be as high as 50 Hz. Motion is fundamentally determined by space geodesy as a time series of positions relative to a global reference frame. Precise timing of the sampled positions in a global time-scale (< 0.1 μ s UTC in even the most basic form of GPS and < 0.1 ns for geodetic GPS) is an added bonus for some applications, such as seismology and SLR.

- Space geodetic surveys are more cost-efficient than classical methods; thus, more points can be surveyed over a larger area than was previously possible.

The benefits that space geodesy could bring to geophysics are precisely the reason why space geodetic methods were developed. For example, NASA's interest in directly observing the extremely slow motions (centimeters per year) caused by plate tectonics was an important driver in the development of SLR, geodetic VLBI, and geodetic GPS (Smith and Turcotte, 1993). SLR was initially a NASA mission dedicated to geodesy. VLBI and GPS were originally developed for other purposes (astronomy and navigation, respectively), though with some research and development (motivated by the potential geophysical reward) they were adapted into high-precision geodetic techniques for geophysical research.

The following are just a few examples of geophysical applications of space geodesy:

- Plate tectonics, by tracking the relative rotations of clusters of space geodetic stations on different plates.
- Interseismic strain accumulation, by tracking the relative velocity between networks of stations in and around plate boundaries.
- Earthquake rupture parameters, by inverting measurements of coseismic displacements of stations located within a few rupture lengths of the fault.
- Postseismic processes and rheology of the Earth's topmost layers, by inverting the decay signature (exponential, logarithmic, etc.) of station positions in the days to decades following an earthquake.
- Magmatic processes, by measuring time variation in the position of stations located on volcanoes or other regions of magmatic activity, such as hot spots.
- Rheology of the Earth's mantle and ice-sheet history, by measuring the vertical and horizontal velocities of stations in the area of postglacial rebound (glacial isostatic adjustment).
- Mass redistribution within the Earth's fluid envelope, by measuring time variation in the Earth's shape, the velocity of the solid Earth's center of mass, the Earth's gravitational field, and the Earth's rotation in space.
- Global change in sea level, by measuring vertical movement of the solid Earth at tide gauges, by measuring the position of spaceborne altimeters in a global reference frame, and by inferring exchange of water between the oceans and continents from mass redistribution monitoring.
- Hydrology of aquifers by monitoring aquifer deformation inferred from time variation in 3-D coordinates of a network of stations on the surface above the aquifer.
- Providing a global reference frame for consistent georeferencing and precision time tagging of nongeodetic measurements and sampling of the Earth, with applications in seismology, airborne and spaceborne sensors, and general fieldwork.

What characterizes modern space geodesy is the broadness of its application to almost all branches of geophysics and the pervasiveness of geodetic instrumentation and data used by geophysicists who are not necessarily experts in geodesy. GPS provides easy access to the global reference frame, which in turn fundamentally depends on the complementary benefits of

all space geodetic techniques (Herring and Perlman, 1993). In this way, GPS provides access to the stability and accuracy inherent in SLR and VLBI without the need for coordination on the part of the field scientist. Moreover, GPS geodesy has benefited tremendously from earlier developments in SLR and VLBI, particularly in terms of modeling the observations.

3.11.1.4 Lunar Laser Ranging Development

Geodesy was launched into the space age by LLR, a pivotal experiment in the history of geodesy. The basic concept of LLR is to measure the distance to the Moon from an Earth-based telescope by timing the flight of a laser pulse that is emitted by the telescope, reflects off the Moon's surface, and is received back into the same telescope. LLR was enabled by the Apollo 11 mission in July 1969, when Buzz Aldrin deployed a laser retroreflector array on the Moon's surface in the Sea of Tranquility (Dickey et al., 1994). Later, Apollo 14 and 15 and a Soviet Lunokhod mission carrying French-built retroreflectors have expanded the number of sites on the Moon. Since initial deployment, several LLR observatories have recorded measurements around the globe, although most of the routine observations have been made at only two observatories: McDonald Observatory in Texas, the United States, and the CERGA station in France. Today, the McDonald Observatory uses a 0.726 m telescope with a frequency-doubled neodymium-doped-YAG laser, producing 1500 mJ pulses of 200 ps width at 532 nm wavelength, at a rate of 10 Hz.

The retroreflectors on the lunar surface are corner cubes, which have the desirable property that they reflect light in precisely the opposite direction, independent of the angle of incidence. Laser pulses take between 2.3 and 2.6 s to complete the 385 000 km journey. The laser beam width expands from 7 mm on Earth to several km at the Moon's surface (a few km), and so in the best conditions, only one photon of light will return to the telescope every few seconds. By timing the flight of these single photons, ranges to the Moon can now be measured with a precision approaching 1 cm.

The LLR experiment has produced the following important research findings fundamental to geophysics (Williams et al., 2001, 2004), all of which represent the most stringent tests to date:

- The Moon is moving radially away from the Earth at 38 mm year^{-1} , an effect attributed to tidal friction, which slows down the Earth's rotation, hence increasing the Moon's distance so as to conserve angular momentum of the Earth–Moon system.
- The Moon likely has a liquid core.
- The Newtonian gravitational constant G is stable to $< 10^{-12}$.
- Einstein's theory of general relativity correctly explains the Moon's orbit to within the accuracy of LLR measurements. For example, the equivalence principle is verified with a relative accuracy of 10^{-13} , and geodetic precession is verified to within $< 0.2\%$ of general relativistic expectations.

3.11.1.5 Satellite Laser Ranging Development

SLR was developed in parallel with LLR and is based on similar principles, with the exception that the retroreflectors (corner

cubes) are placed on artificial satellites (Degnan, 1993). Experiments with SLR began in 1964 with NASA's launch of the Beacon-B satellite, tracked by Goddard Space Flight Center with a range accuracy of several meters. Following a succession of demonstration tests, operational SLR was introduced in 1975 with the launch of the first dedicated SLR satellite, Starlette, launched by the French Space Agency, soon followed in 1976 by NASA's Laser Geodynamics Satellite (LAGEOS-1) in a near-circular orbit of 6000 km radius. Since then, other SLR satellites now include LAGEOS-II, Stella, Etalon-1 and -2, and AJISAI. There are now approximately ten dedicated satellites that can be used as operational SLR targets for a global network of more than 40 stations, most of them funded by NASA for purposes of investigating geodynamics, geodesy, and orbital dynamics (Tapley et al., 1993).

SLR satellites are basically very dense reflecting spheres orbiting the Earth. For example, LAGEOS-II launched in 1992 is a 0.6 m sphere of mass 411 kg. The basic principle of SLR is to time the round-trip flight of a laser pulse shot from the Earth to the satellite. Precise time tagging of the measurement is accomplished with the assistance of GPS. The round-trip time of flight measurements can be made with centimeter-level precision, allowing for the simultaneous estimation of the satellite orbits, gravitational field parameters, tracking station coordinates, and Earth rotation parameters. The reason the satellites have been designed with a high mass to surface area ratio is to minimize accelerations due to nonconservative forces such as drag and solar radiation pressure. This produces a highly stable and predictable orbit and hence a stable dynamic frame from which to observe the Earth's rotation and station motions.

SLR made early contributions to the confirmation of the theory of plate tectonics (Smith et al., 1993) and toward measuring and understanding contemporary crustal deformation in plate boundary zones (Jackson et al., 1994; Wilson and Reinhart, 1993). To date, SLR remains the premier technique for determining the location of the center of mass of the Earth system and its motion with respect to the Earth's surface (Chen et al., 1999; Ray, 1998; Watkins and Eanes, 1997). As an optical technique that is relatively less sensitive to water vapor in the atmosphere, SLR has also played a key role in the realization of reference frame scale (Dunn et al., 1999). The empirical realization of scale and origin is very important for the testing of dynamic Earth models within the rigorous framework of the International Terrestrial Reference System (ITRS) (McCarthy, 1996).

Today, SLR is used in the following research (Perlman et al., 2002):

- Mass redistribution in the Earth's fluid envelope, allowing for the study of atmosphere–hydrosphere–cryosphere–solid Earth interactions. SLR can sense the Earth's changing gravitational field (Bianco et al., 1997; Cheng and Tapley, 1999, 2004; Gegout and Cazenave, 1993; Nerem et al., 1993; Devoti et al., 2001), the location of the solid Earth's center of mass with respect to the center of mass of the entire Earth system (Chen et al., 1999). Also, SLR determination of the Earth's rotation in the frame of the stable satellite orbits reveals the exchange of angular momentum between the solid Earth and fluid components of the Earth

system (Chao et al., 1987). SLR stations can sense the deformation of the Earth's surface in response to loading of the oceans, atmosphere, and hydrosphere and can infer mantle dynamics from response to the unloading of ice from past ice ages (Argus et al., 1999).

- Long-term dynamics of the solid Earth, oceans, and ice fields (Sabadini et al., 2002). SLR can sense surface elevations unambiguously with respect to the Earth's center of mass, such as altimeter satellite height and hence ice-sheet and sea surface height. Thus, SLR is fundamental to the terrestrial reference frame and the long-term monitoring of sea level change.
- Mantle–core interaction through long-term variation in the Earth's rotation (Eubanks, 1993).
- General relativity, specifically the Lense–Thirring effect of frame dragging (Cuifolini and Pavlis, 2004).

SLR is a relatively expensive and cumbersome technique and so has largely been superseded by the GPS technique for most geophysical applications. SLR is still necessary for maintaining the stability of the International Terrestrial Reference Frame (ITRF), in particular, to aligning the ITRF origin with the specifications of ITRS (Altamimi et al., 2002). SLR is also necessary to determine long-term variation in the low-degree components of the Earth's gravitational field. SLR is maintained by NASA to support high-precision orbit determination (such as for satellite altimetry), though GPS is also now being used for that purpose.

3.11.1.6 VLBI Development

VLBI, originally a technique designed for observing distant celestial radio sources with high angular resolution, was from the late 1970s developed for high-precision geodetic applications by applying the technique 'in reverse' (Rogers et al., 1978). Much of this development of geodetic VLBI was performed by the NASA Crustal Dynamics Project initiated in 1979 (Bosworth et al., 1993) with the idea to have an alternative technique to SLR to provide independent confirmation of scientific findings.

Conceptually, geodetic VLBI uses radio waves from distant quasars at known positions on the celestial sphere and measures the difference in the time of arrival of signals from those quasars at stations (radio observatories) on the Earth's surface. Such data provide information on how the geometry of a network of stations evolves in time. This time-variable geometry can be inverted to study geophysical processes such as the Earth's rotation and plate tectonics and can be used to define a global terrestrial reference frame with high precision. Unique to VLBI is that it can provide an unambiguous, stable tie between the orientation of the terrestrial reference frame and the celestial reference frame, that is, Earth orientation. However, as a purely geometric technique, it is not directly sensitive to the Earth's center of mass and gravitational field, although inferences by VLBI on gravity can be made through models that connect gravity to Earth's shape, such as tidal and loading models.

Comparisons between VLBI and SLR proved to be important for making improvements in both methods. As a radio technique, VLBI is more sensitive to errors in atmospheric

refraction (Davis et al., 1985; Niell, 1996; Truehaft and Lanyi, 1987) than the optical SLR technique; however, VLBI has the advantage that the sources are quasars that appear to be essentially fixed in the sky, thus providing the ultimate in celestial reference frame stability. VLBI is therefore the premier technique for determining parameters describing the Earth rotation's in inertial space, namely, precession, nutation, and UT1 (the angle of rotation with respect to UTC) (Eubanks, 1993). VLBI ultimately has proven to be more precise than SLR in measuring distances between stations.

However, VLBI has never been adapted for tracking Earth-orbiting platforms and is highly insensitive to the Earth's gravitational field and thus cannot independently realize the Earth's center of mass as the origin of the global reference frame. On the other hand, the stability of scale in VLBI is unsurpassed. For most geophysical applications, GPS has superseded VLBI, except for the important reference frame and Earth orientation tasks described earlier. VLBI remains important for characterizing long-wavelength phenomena such as postglacial rebound, with the highest precision among all techniques today, and therefore is integral to the stability of global terrestrial reference frames.

To summarize, geodetic VLBI's main contributions to scientific research involve (Schlueter et al., 2002)

- unambiguous Earth orientation parameters, which can be used to study angular momentum exchange between the solid Earth and its fluid reservoirs and provides a service to astronomy and space missions by connecting the terrestrial reference frame to the celestial reference frame (Eubanks, 1993);
- providing a stable scale for the global terrestrial reference frame (Boucher and Altamimi, 1993);
- providing the highest-precision measurements of long-wavelength Earth deformations, thus providing stability to the global frame, and constraints on large-scale geodynamics such as postglacial rebound and plate tectonics (Argus et al., 1999; Stein, 1993).

3.11.1.7 Global Positioning System Development

As of September 2006, the GPS consists of 29 active satellites that can be used to position a geodetic receiver with an accuracy of millimeters within the ITRF. To do this requires geodetic-class receivers (operating at two frequencies, and with antennas designed to suppress signal multipath), currently costing a few thousand US dollars, and geodetic research-class software (developed by various universities and government institutions around the world). Such software embody leading-edge models (of the solid Earth, atmosphere, and satellite dynamics) and data processing algorithms (signal processing and stochastic parameter estimation). Many of the models have been developed as a result of much research conducted by the international geodetic and geophysical community, often specifically to improve the accuracy of GPS. Today, it is even possible for a nonexpert to collect GPS data and produce receiver positions with centimeter accuracy by using an Internet service for automatic data processing.

The geodetic development of the GPS has been driven by a number of related factors (Blewitt, 1993):

- The foundation for many of the research-class models was already in place owing to the similarities between GPS and VLBI (as radio techniques) and GPS and SLR (as satellite dynamic techniques), thus giving an early boost to GPS geodesy. Continued collaboration with the space geodetic community has resulted in standard models such as those embodied by the ITRS Conventions (McCarthy, 1996), which aim to improve the accuracy and compatibility of results from the various space geodetic techniques.
- GPS is of relatively low cost and yet has comparable precision to VLBI and SLR. Whereas the GPS itself is paid for by the US taxpayer, the use of the system is free to all as a public good. This has made GPS accessible to university researchers, and the resulting research has further improved GPS accuracy through better models.
- GPS stations are easy to deploy and provide a practical way to sample the deformation field of the Earth's surface more densely, thus allowing space geodesy to address broader diversity scientific questions. This has opened up interdisciplinary research within geophysics, leading to discoveries in unforeseen areas and to further improvements in GPS accuracy through improved observation models.
- GPS was readily adopted because of the ease of access to the ITRF on an ad hoc basis, without the need for special global coordination from the point of view of an individual investigator. Furthermore, the ITRF gives implicit access to the best possible accuracy and stability that can be achieved by SLR and VLBI (Herring and Pearlman, 1993).

Following closely the historical perspectives of Evans et al. (2002) and Blewitt (1993), GPS has its roots as a successor to military satellite positioning systems developed in the 1960s, though the first geophysical applications of GPS were not realized until the early 1980s. In the run-up to the space age in 1955, scientists at the Naval Research Laboratory first proposed the application of satellite observations to geodesy. By optical observation methods, the first geodetic satellites were quickly used to refine parameters of the Earth's gravitational field. Optical methods were eventually made obsolete by the Doppler technique employed by the Navy Navigation Satellite System (TRANSIT). As the name implies, Doppler positioning was based on measuring the frequency of the satellite signal as the relative velocity changed between the satellite and the observer. By the early 1970s, Doppler positioning with 10 m accuracy became possible on the global scale, leading to the precise global reference frame 'World Geodetic System 1972' (WGS 72), further improved by WGS 84, which was internally accurate at the 10 cm level. Having a global network of known coordinates together with the success of radiometric tracking methods set the stage for the development of a prototype GPS in the late 1970s.

The US Department of Defense launched its first prototype Block I GPS satellite, NAVSTAR 1, in February 1978. By 1985, ten more Block 1 satellites had been launched, allowing for the development and testing of prototype geodetic GPS data processing software that used dual-frequency carrier phase observables. In February 1989, the first full-scale operational GPS satellite known as Block II was deployed, and by January 1994, a nominally full constellation of 24 satellites was completed, ensuring that users could see satellites of a sufficient

number (at least 5) at anytime, anywhere in the world. Initial operational capability was officially declared in December 1993, and full operational capability was declared in April 1995. From July 1997, Block IIRs began to replace GPS satellites. The first modified version Block IIR-M satellite was launched in 2005 (for the first time emitting the L2C signal, which allows civilian users to calibrate for ionospheric delay). The current constellation of 29 satellites includes extra satellites as 'active spares' to ensure seamless and rapid recovery from a satellite failure. The first Block IIF satellite was scheduled to launch in 2008 and may transmit a new civil signal at a third frequency.

The GPS design built on the success of Doppler by enabling the measurement of a biased range ('pseudorange') to the satellite, which considerably improved positioning precision. Carrier phase tracking technology further improved the signal measurement precision to the few millimeter level. As a radio technique, VLBI technology was adapted in NASA's prototype geodetic GPS receivers. The SERIES receiver, developed by MacDoran (1979) at the Jet Propulsion Laboratory (JPL), pointed at one source at a time using a directional antenna (a technique no longer used). Many key principles and benefits of the modern GPS geodesy were based on the omnidirectional instrument, MITES, proposed by Counselman and Shapiro (1979). This was developed by the Massachusetts Institute of Technology (MIT) group into the Macrometer instrument, which provided centimeter-level accuracy using the innovative double-difference method for eliminating clock bias, a method that has its origins in radio navigation of the Apollo mission (Counselman et al., 1972).

By the mid 1980s, commercial receivers such as the Texas Instrument TI 4100 became available (Henson et al., 1985) and were quickly deployed by geophysicists in several pioneering experiments to measure the slow motions associated with plate tectonics (Dixon et al., 1985; Freymueller and Kellogg, 1990; Prescott et al., 1989); such experiments spurred the development of analysis techniques to improve precision at the level required by geophysics (Larson and Agnew, 1991; Larson et al., 1991; Tralli et al., 1988). Important developments during these early years include ambiguity resolution over long distances (Blewitt, 1989; Dong and Bock, 1989), precise orbit determination (Beutler et al., 1985; King et al., 1984; Lichten and Border, 1987; Swift, 1985), and troposphere modeling (Davis et al., 1987; Lichten and Border, 1987; Tralli and Lichten, 1990).

The development of geodetic GPS during the 1980s was characterized by intensive hardware and software development with the goal of sub-centimeter positioning accuracy, over increasingly long distances. A prototype digital receiver known as 'Rogue' was developed by the JPL (Thomas, 1988), which produced high-precision pseudorange data that could be used to enhance data processing algorithms, such as ambiguity resolution. Several high-precision geodetic software packages that were developed around this time are still in use and far exceed the capabilities of commercial packages. These included the Bernese developed at the University of Bern (Beutler et al., 1985; Gurtner, 1985; Rothacher et al., 1990), GAMIT-GLOBK developed at MIT (Bock et al., 1986; Dong and Bock, 1989; Herring et al., 1990), and GIPSY-OASIS developed at JPL (Blewitt, 1989, 1990; Lichten and Border, 1987; Sovers and Border, 1987).

GPS became fully operational in 1994, with the completion of a full constellation of 24 satellites. Developments toward high precision in the 1990s include (1) truly global GPS solutions made possible by the completion of the Block II GPS constellation and, simultaneously, installation and operation of the global network in 1994 (shown in its current configuration in [Figure 2](#)) by the International GPS Service (IGS, since renamed the International GNSS Service) ([Beutler et al., 1994a](#)); (2) global-scale ambiguity resolution ([Blewitt and Lichten, 1992](#)); (3) further refinement to tropospheric modeling and the inclusion of tropospheric gradient parameters ([Bar-Sever et al., 1998](#); [Chen and Herring, 1997](#); [Davis et al., 1993](#); [McMillan, 1995](#); [Niell, 1996](#); [Rothacher et al., 1998](#)); (4) adoption of baseband-digital GPS receivers with the low-multipath choke ring antenna developed originally at JPL ([Meehan et al., 1992](#)), which remains the IGS standard design today; (5) improved orbit models, particularly with regard to GPS satellite attitude, and the tuning of stochastic models for solar radiation pressure ([Bar Sever, 1996](#); [Beutler et al., 1994b](#); [Fliegel and Gallini, 1996](#); [Fliegel et al., 1992](#); [Kuang et al., 1996](#)); (6) improved reference system conventions ([McCarthy, 1996](#)); and (7) simultaneous solution for both orbits and station positions (fiducial-free global analysis) ([Heflin et al., 1992](#)).

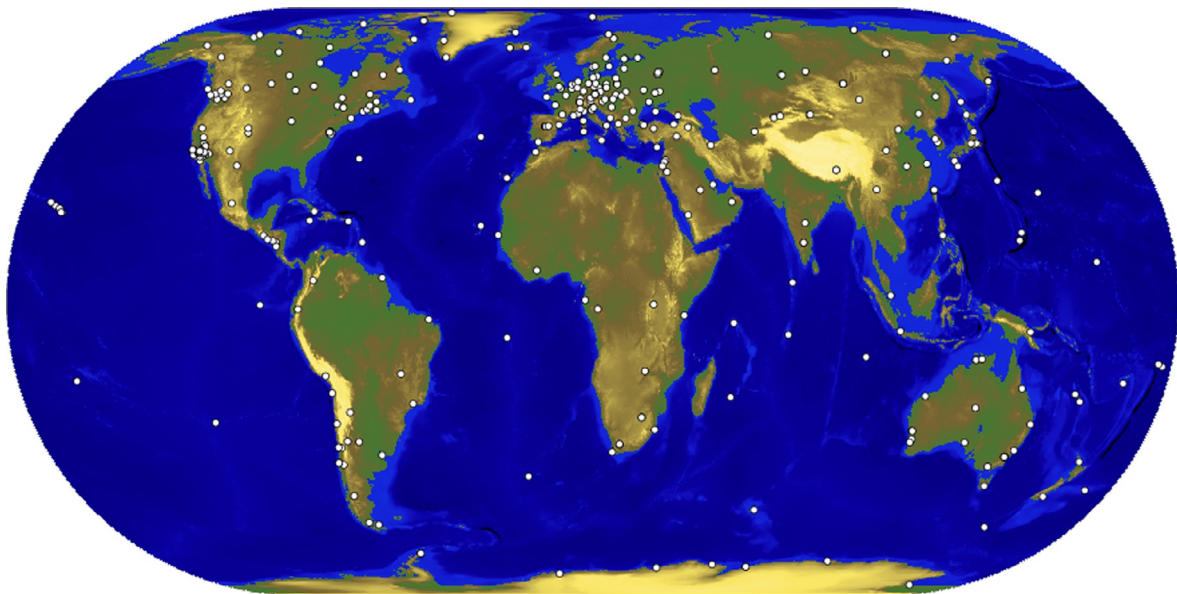
The focus of developments in the decade includes (1) building on earlier work by [Schupler et al. \(1994\)](#), antenna phase center variation modeling and calibrations for both stations and the GPS satellites themselves ([Ge et al., 2005](#); [Mader, 1999](#); [Mader and Czopek, 2002](#); [Schmid and Rothacher, 2003](#); [Schmid et al., 2005](#)); (2) densification of stations in the ITRF and the installation of huge regional networks of geodetic GPS stations, such as the ~1000 station Plate Boundary Observatory currently being installed in the western North America ([Silver et al., 1999](#)); (3) improved analysis of large regional networks of stations through

common-mode signal analysis ([Wdowinski et al., 1997](#)) and faster data processing algorithms ([Bertiger et al., 2010](#); [Zumberge et al., 1997](#)); (4) the move toward real-time geodetic analysis with applications such as GPS seismology ([Larson et al., 2003](#); [Nikolaidis et al., 2001](#)) and tsunami warning systems ([Blewitt et al., 2006](#)), including signal processing algorithms to filter out sidereally repeating multipath ([Bock et al., 2000, 2004](#); [Choi et al., 2004](#)); and (5) further improvements in orbit determination ([Ziebart et al., 2002](#)), tropospheric modeling ([Boehm et al., 2006](#)), and higher-order ionospheric models ([Kedar et al., 2003](#)).

With the significant improvements to modeling since the inception of the IGS in 1994, data reprocessing of global GPS data sets has begun in earnest. Early results indicate superior quality of the GPS data products, such as station coordinate time series, orbit and clock accuracy, and Earth orientation parameters ([Steinberger et al., 2006](#)).

3.11.1.8 Comparing GPS with VLBI and SLR

GPS geodesy can be considered a blend of the two earlier space geodetic techniques: VLBI and SLR. The most obvious similarities are that (1) SLR and GPS are satellite systems and so are sensitive to Earth's gravitational field and (2) VLBI and GPS are radio techniques and so the observables are subject to atmospheric refraction in a similar way. Due to these similarities, GPS geodesy has benefited from earlier work on both VLBI and SLR observation modeling and from reference system conventions already established through a combination of astronomical observation, VLBI and SLR observation, and geodynamic modeling. Moreover, Earth models such as tidal deformation are required by all global geodetic techniques, so GPS geodesy was in a position to exploit what had already been learned. Today, the improvements in modeling any of the techniques can often be exploited by another technique.



IGS 2006 Dec 30 17:22:57

Figure 2 The global network of the International GPS Service. Courtesy of A. Moore.

The similarities between certain aspects of the different techniques lead to an overlap of strengths and weaknesses, error sources, and sensitivity to geophysical parameters of interest. The strengths and weaknesses can be summarized as follows:

- The main strength of SLR is the stability of the orbits due to custom-designed satellites. This leads to high sensitivity to the low-degree gravitational field harmonics and their long-term changes in time. This includes the degree-one term (characterizing geocenter motion, the motion of the solid Earth with respect to the center of mass of the entire Earth system), which is important for realizing the origin of the ITRF. As an optical technique, SLR is insensitive to moisture in the atmosphere and so has relatively small systematic errors associated with signal propagation. This inherently leads to more robust estimation of station height. On the other hand, SLR has problems working during daylight hours and in cloudy conditions. It is also an expensive and bulky technique and so suffers from a lack of geographic coverage.
- The main strength of VLBI is the stability and permanency of the sources, which are quasars. This leads to two important qualities: (1) VLBI is insensitive to systematic error in orbit dynamic models and can potentially be the most stable system for detecting the changes over the longest observed time periods, and (2) VLBI is strongly connected to an external, celestial reference frame, a vantage point from which Earth orientation and rotation can be properly determined. A major weakness of VLBI is (similar to SLR) its expensiveness and bulkiness. Moreover, some VLBI observatories are used for astronomical purposes and so cannot be dedicated to continuous geodetic measurement. VLBI antennas are very large structures that have their own set of problems, including the challenge to relate the observations to a unique reference point, and the stability of the structure with respect to wind and gravitational stress, and aging.

The main advantage of GPS is its low cost and ease of deployment and all-weather capability. Thus, GPS can provide much better geographic coverage, continuously. The flexibility of deployment allows for ties to be made between the terrestrial reference frames of the various techniques through collocation at SLR and VLBI sites. The disadvantage of GPS is that it is subject to both the systematic error associated with orbit dynamics and atmospheric moisture. Furthermore, the omnidirectional antennas of GPS lead to multipath errors. Thus, geodetic GPS is essential for improved sampling of the Earth in time and space but ultimately depends on SLR and VLBI to put such measurements into a reference frame that has long-term stability. This synergy lies at the heart of the emerging concept GGOS, the Global Geodetic Observing System, under the auspices of the International Association of Geodesy (IAG) (Rummel et al., 2005).

3.11.1.9 GPS Receivers in Space: LEO GPS

GPS has proved extremely important for positioning spaceborne scientific instruments in low-Earth orbit (sometimes called LEO GPS). Evans et al. (2002) provided an overview of

spaceborne GPS, which is only briefly summarized here. The Landsat 4 satellite launched in 1982 was the first to carry a GPS receiver, called GPSPAC. This was followed by three more missions using GPSPAC, including Landsat 5 in 1984 and DoD satellites in 1983 and 1984. As the GPS satellite constellation grew during the 1980s, so the precision improved, enabling decimeter-level accuracy for positioning spaceborne platforms. Following Evans et al. (2002), the applications of spaceborne GPS can be categorized as (1) precise orbit determination of the host satellite for applications such as altimetry; (2) measurement of the Earth's gravitational field, such as the missions CHAMP and GRACE; (3) ionospheric imaging; and (4) indirect enhancements to global geodesy and remote sensing. In addition to these categories, spaceborne GPS is also being used to invert for the refractivity of the Earth's neutral atmosphere by occultation measurements, which can be used, for example, to infer stratospheric temperatures for studies of global climate change.

3.11.1.10 Global Navigation Satellite Systems

The success of GPS has led to the development of similar future systems, generically referred to as GNSS. To achieve global coverage, each GNSS system generally has a constellation of 20–30 satellites in roughly 12 h orbits. Some systems are augmented with a few satellites in either geostationary or inclined geosynchronous orbit.

The Russian system GLONASS (a Russian acronym that literally translates to GNSS) was actually developed in parallel with GPS and achieved global coverage with 24 satellites in orbit by 1995. After a subsequent period of degradation, the GLONASS system was restored back to a full constellation of 24 satellites by the end of 2011 and, as of 2013, has 29 satellites in orbit. Many modern GNSS receivers can track both GPS and GLONASS. Like GPS, the GLONASS satellite orbits and clocks are modeled by the IGS. However, in part due to the different transmission frequencies of the GLONASS satellites, which hinder the application of carrier phase ambiguity resolution techniques, the system has not proven to deliver geodetic solutions with such high precision as GPS. Nevertheless, GLONASS data can enhance GPS in situations where the sky is not completely visible, such as in an urban canyon environment.

An example of a GNSS under development is the European Galileo system, which has been scheduled to have full operational capability with 30 satellites before 2020, following several years of initial operational capability. By October 2012, four Galileo satellites had become operational, enabling the first production of 3-D position solutions.

The Chinese experimental regional BeiDou Navigation Satellite System (BDS) of five geostationary satellites is being expanded to have global coverage. BDS plans to add 30 non-geostationary satellites to the constellation, including three that are in inclined geosynchronous orbit. By 2013, BDS had 15 operational satellites and is planned to have a full global constellation by 2020.

Regional enhancement systems are being developed too. In Japan, the Quasi-Zenith Satellite System (QZSS) is planned to have three satellites in inclined geosynchronous orbit to enhance GPS in that region. As of 2012, one QZSS satellite

was in operation. Similarly, the Indian Regional Navigation Satellite System (IRNSS) is planned to have seven satellites to augment GPS (with three in geostationary orbit and four in inclined geosynchronous orbit), with the first launch planned for summer 2013.

The main reason for the development of alternative systems to GPS is to ensure access to GNSS signals that are not under the control of any single nation, with implications for the military in times of war and national emergencies and for civilian institutions such as national aviation authorities that have stringent requirements on guaranteed access to a sufficient number of GNSS signals at all times.

Thus, the future of GNSS is essentially guaranteed. By analogy with the Internet, navigation and geospatial referencing has become such an embedded part of the world's infrastructure and economy that it is now difficult to imagine a future world where GNSS is not pervasive. As GPS has proved, a GNSS system does not necessarily have to be designed with high-precision geodesy in mind in order for it to be used successfully as a high-precision geophysical tool. However, it is likely that future GNSS systems will take more into account the high-precision applications in their design and thus may be even better suited to geophysical applications than GPS currently is. Much can be done to mitigate errors, for example, in the calibration of the phase center variation in the satellite transmitting antenna or the transmission of signals at several different frequencies.

Satellite geodesy in the future will therefore use multiple GNSS systems interoperably and simultaneously. This will lead to improved precision and robustness of solutions. It will also allow for new ways to probe and hopefully mitigate systematic errors associated with specific GNSS systems and satellites. The continued downward spiral in costs of GNSS receiver systems will undoubtedly result in the deployment of networks with much higher density (reduced station spacing), which will benefit geophysical studies. For example, it would allow for higher-resolution determination of strain accumulation due to crustal deformation in plate boundary zones.

3.11.1.11 International GNSS Service

Infrastructure development and tremendous international cooperation characterized the 1990s. GPS operations moved away from the campaigns, back to the model of permanent stations, familiar to VLBI and SLR. As the prototype receivers developed by research groups in the 1980s had become commercialized, the cost of installing a GPS station in the 1990s had fallen to ~\$25 K, in contrast to the millions of dollars required for VLBI/SLR. Thus, the long-range goal of the federal funding agencies was realized: dozens of GPS stations could be installed for the price of one VLBI station.

With the cooperation of ~100 research institutions around the world under the umbrella of the International GPS (now GNSS) Service (IGS), a global GPS network (now at ~350 stations; Figure 2) with a full geodetic analysis system came into full operation in 1994 (Beutler et al., 1994a). This backbone, together with the regional stations located in areas of tectonic activity, such as Japan and California, forms a global-scale instrument capable of resolving global plate tectonic motions and regional phenomena such as earthquake

displacement. As a result of this international cooperation, a culture of data sharing has developed, with data freely available for research purposes via the Internet from IGS Global Data Centers. The establishment of a standard GPS measurement format known as RINEX (Receiver Independent Exchange) has facilitated this extensive exchange of data through IGS (see Table 1 for IGS data availability).

The mission of the IGS is to provide the highest-quality data and products as the standard for GNSS in support of Earth science research and multidisciplinary applications. So although the IGS does not specifically carry out geophysical investigations, it does provide an essential service without which such investigations would be very costly and difficult to carry out. The 1990s has seen the development of collaborations with specific geophysical goals. Groups such as WEGENER (Plag et al., 1998) and UNAVCO (<http://www.unavco.org>) have provided an umbrella for geoscientists using GPS geodesy as a tool. Such groups depend on IGS for their success; conversely, IGS as a volunteer organization depends on such users to contribute to its operations and technical working groups.

The infrastructure has indeed become quite complex, yet cooperative, and often with an efficient division between geodetic operations and geodynamic investigations. As an example of how infrastructure is developing, solutions are being exchanged in a standard Software INdependent EXchange (SINEX) format to enable the construction of combined network solutions and, therefore, combined global solutions for Earth surface kinematics. This standard has since also been adopted by the other space geodetic techniques. Combination solutions have the advantage that (1) the processing burden is distributed among many groups who can check each other's solutions, (2) noise and errors are reduced through increased redundancy and quality control procedures, (3) coverage and density are increased, and (4) regional geodynamics can be interpreted in a self-consistent global context. An emerging focus of this decade (2000s) is the development of such combination solutions, and on the inversion of these solutions to infer geophysical parameters.

As the premier service for high-precision geodesy, the quality of IGS products is continually improving with time (Figure 3) and represents the current state-of-the-art (Dow

Table 1 IGS raw data types and availability

	<i>Latency</i>	<i>Updates</i>	<i>Sample interval</i>
<i>Ground observations</i>			
GPS and GLONASS data	1 day	Daily	30 s
	1 h	Hourly	30 s
	15 min	15 min	1 s ^a
GPS broadcast ephemerides	1 day	Daily	N/A
	1 h	Hourly	
	15 min	15 min	
GLONASS broadcast ephemerides	1 day	Daily	N/A
Meteorologic	1 day	Daily	5 min
	1 h	Hourly	5 min
<i>Low-Earth orbiter observations</i>			
GPS	4 days	Daily	10 s

^aSelected subhourly stations have sampling intervals $1\text{ s} < t < 10\text{ s}$.

Source: IGS Central Bureau, <http://igs.cb.jpl.nasa.gov>.

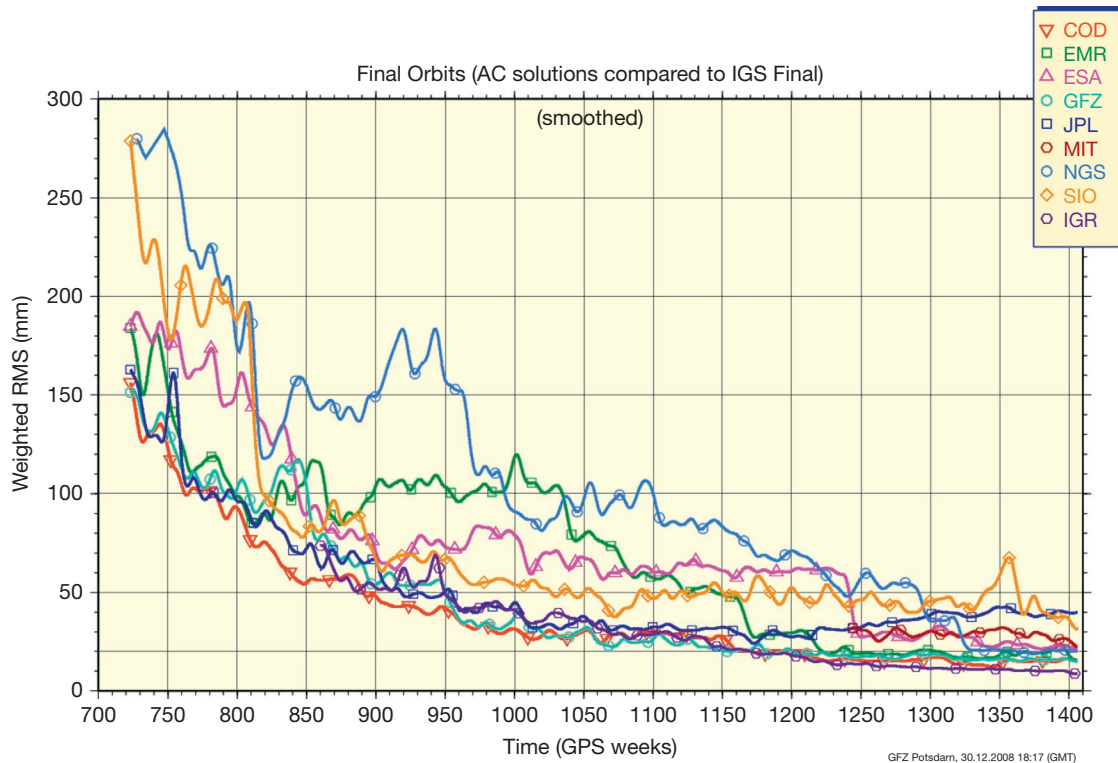


Figure 3 Plot showing the improvement of IGS orbit quality with time. Courtesy of G. Gendt.

et al., 2005b; Moore, 2007). The levels of accuracy claimed by the IGS for its various products are reproduced in Table 2.

Analogous to the IGS, geodetic techniques are organized as scientific services within the IAG. The IAG services are as follows:

- International Earth Rotation and Reference Systems Service (IERS) (IERS, 2004).
- International GNSS Service, formerly the International GPS Service (IGS) (Dow et al., 2005b).
- International VLBI Service (IVS) (Schlüter et al., 2002).
- International Laser Ranging Service (ILRS) (Pearlman et al., 2002).
- International DORIS Service (IDS) (Tavernier et al., 2005).

These scientific services, as well as gravitational field services and an expected future altimetry service, are integral components of the future 'Global Geodetic Observing System' (GGOS) (Rummel et al., 2005; <http://www.ggos.org>). Closer cooperation and understanding through GGOS are expected to bring significant improvements to the ITRF and to scientific uses of geodesy in general (Dow et al., 2005a).

Figure 4 shows the current status of collocated space geodetic sites, which forms the foundation for ITRF and GGOS. Collocation is essential to exploit the synergy of the various techniques, and so increasing the number and quality of collocated sites will be a high priority for GGOS. In addition, the IGS adapts to incorporate new GNSS systems as they come online.

3.11.2 GPS and Basic Principles

3.11.2.1 Basic Principles

GPS positioning is based on the principle of 'trilateration,' which is the method of determining position by measuring distances to points of known positions (not to be confused with triangulation, which measures angles between known points). At a minimum, trilateration requires three ranges to three known points. In the case of GPS, the known points would be the positions of the satellites in view. The measured ranges would be the distances between the GPS satellites and a user's GPS receiver. (Note that GPS is a completely passive system from which users only receive signals.) GPS receivers, on the other hand, cannot measure ranges directly, but rather 'pseudoranges.' A pseudorange is a measurement of the difference in time between the receiver's local clock and an atomic clock on board a satellite. The measurement is multiplied by the speed of light to convert it into units of range (meters):

$$\text{pseudorange} = (\text{receiver_time} - \text{satellite_time}) \times \text{speed_of_light} \quad [1]$$

The satellite effectively sends its clock time by an encoded microwave signal to a user's receiver. It does this by multiplying a sinusoidal carrier wave by a known sequence ('code') of +1 and -1, where the timing of the signal (both code and carrier wave) is controlled by the satellite clock. The receiver generates an identical replica code and then performs a cross

Table 2 IGS (and broadcast) product availability and quality

		Accuracy ^a	Latency	Updates	Interval
<i>GPS satellite ephemerides</i>					
Broadcast ^b	Orbits	160 cm	Real time	N/A	N/A
	Satellite clocks	7 ns			
Ultrarapid (predicted half)	Orbits	10 cm	Real time	6 h	15 min
	Satellite clocks	5 ns			
Ultrarapid (observed half)	Orbits	<5 cm	3 h	6 h	15 min
	Satellite clocks	0.2 ns			
Rapid	Orbits	<5 cm	17 h	Daily	15 min
	All clocks	0.1 ns			5 min
Final	Orbits ^c	<5 cm	13 days	Weekly	15 min
	All clocks ^d	0.1 ns			5 min
<i>GLONASS satellite ephemerides</i>					
Final		15 cm	2 weeks	Weekly	15 min
<i>IGS station coordinates^e</i>					
Positions	Horizontal	3 mm	12 days	Weekly	Weekly
	Vertical	6 mm			
Velocities	Horizontal	2 mm year ⁻¹	12 days	Weekly	~Years
	Vertical	3 mm year ⁻¹			
<i>Earth rotation parameters^f</i>					
Ultrarapid (predicted half)	Pole position	0.3 mas	Real time	6 h	6 h
	Pole rate	0.5 mas day ⁻¹			
	Length of day	0.06 ms			
Ultrarapid (observed half)	Pole position	0.1 mas	3 h	6 h	6 h
	Pole rate	0.3 mas day ⁻¹			
	Length of day	0.03 ms			
Rapid	Pole position	<0.1 mas	17 h	Daily	Daily
	Pole rate	<0.2 mas day ⁻¹			
	Length of day	0.03 ms			
Final	Pole position	0.05 mas	13 days	Weekly	Daily
	Pole rate	<0.2 mas day ⁻¹			
	Length of day	0.02 ms			

^aGenerally, precision (based on scatter of solutions) is better than the accuracy (based on comparison with independent methods).

^bBroadcast ephemerides only shown for comparison (but are also available from IGS).

^cOrbit accuracy based on comparison with satellite laser ranging to satellites.

^dClock accuracy is expressed relative to the IGS timescale, which is linearly aligned to GPS time in 1-day segments.

^eStation coordinate and velocity accuracy based on intercomparison statistics from ITRF.

^fEarth rotation parameters based on intercomparison statistics by IERS. IGS uses VLBI results from IERS Bulletin A to calibrate for long-term LOD biases.

Source: IGS Central Bureau, <http://igs.cb.jpl.nasa.gov>, courtesy of A. Moore.

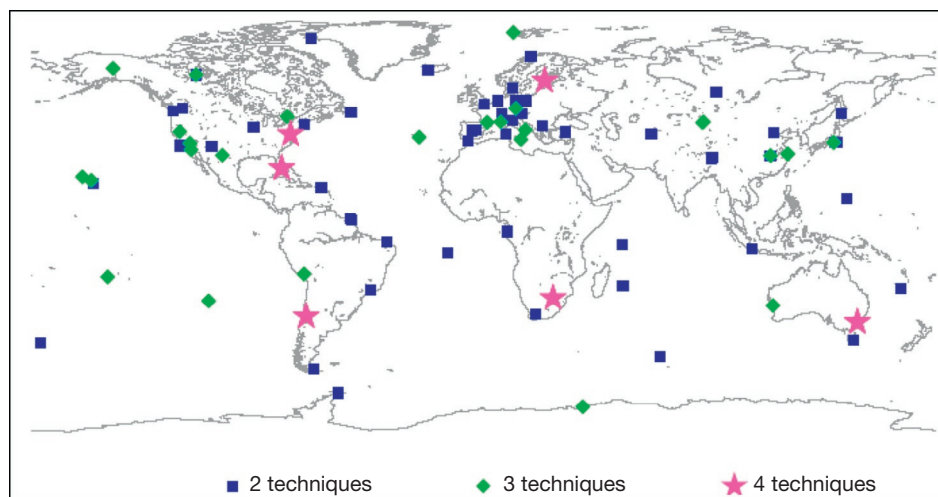


Figure 4 Distribution of collocated space geodetic stations that have at least two different operational techniques of GPS, VLBI, SLR, and DORIS. Courtesy of Z. Altamimi.

correlation with the incoming signal to compute the required time shift to align the codes. This time shift multiplied by the speed of light gives the pseudorange measurement.

The reason the measurement is called a 'pseudorange' is that the range is biased by error in the receiver's clock (typically a quartz oscillator). However, this bias at any given time is the same for all observed satellites, and so it can be estimated as one extra parameter in the positioning solution. There are also (much smaller) errors in the satellites' atomic clocks, but GPS satellites handle this by transmitting another code that tells the receiver the error in its clock (which is routinely monitored and updated by the US Department of Defense).

Putting all this together, point positioning with GPS therefore requires pseudorange measurements to at least four satellites, where information on the satellite positions and clocks is also provided as part of the GPS signal. Three coordinates of the receiver's position can then be estimated simultaneously along with the receiver's clock offset. By this method, GPS positioning with few meter accuracy can be achieved by a relatively low-cost receiver.

Hence, GPS also allows the user to synchronize time to the globally accessible atomic standard provided by GPS. In fact, the GPS atomic clocks form part of the global clock ensemble that define Universal Coordinated Time (UTC). Note that since GPS time began (6 January 1980), there have accumulated a number of leap seconds (16 s as of July 2012) between GPS time (a continuous timescale) and UTC (which jumps occasionally to maintain approximate alignment with the variable rotation of the Earth). Synchronization to GPS time (or UTC) can be achieved to $<0.1 \mu\text{s}$ using a relatively low-cost receiver. This method is suitable for many time-tagging applications, such as in seismology, in SLR, and even for GPS receivers themselves. That is, by using onboard point positioning software, GPS receivers can steer their own quartz oscillator clocks through a feedback mechanism such that observations are made within a certain tolerance of GPS time.

A fundamental principle to keep in mind is that GPS is a timing system. By the use of precise timing information on radio waves transmitted from the GPS satellite, the user's receiver can measure the range to each satellite in view and hence calculate its position. Positions can be calculated at every measurement epoch, which may be once per second when applied to car navigation (and in principle as frequently as 50 Hz). Kinematic parameters such as velocity and acceleration are secondary, in that they are calculated from the measured time series of positions.

3.11.2.2 GPS Design and Consequences

The GPS has three distinct segments:

1. The space segment, which includes the constellation of ~ 30 GPS satellites that transmit the signals from space down to the user, including signals that enable a user's receiver to measure the biased range (pseudorange) to each satellite in view and signals that tell the receiver the current satellite positions, the current error in the satellite clock, and other information that can be used to compute the receiver's position.

2. The control segment (in the US Department of Defense), which is responsible for the monitoring and operation of the space segment, including the uploading of information that can predict the GPS satellite orbits and clock errors into the near future, which the space segment can then transmit down to the user.
3. The user segment, which includes the user's GPS hardware (receivers and antennas) and GPS data processing software for various applications, including surveying, navigation, and timing applications.

The satellite constellation is designed to have at least four satellites in view anywhere, anytime, to a user on the ground. For this purpose, there are nominally 24 GPS satellites distributed in six orbital planes. In addition, there is typically an active spare satellite in each orbital plane, bringing the total number of satellites closer to 30. The orientation of the satellites is always changing, such that the solar panels face the sun and the antennas face the center of the Earth. Signals are transmitted and received by the satellite using microwaves. Signals are transmitted to the user segment at frequencies $L1 = 1575.42 \text{ MHz}$ and $L2 = 1227.60 \text{ MHz}$ in the direction of the Earth. This signal is encoded with the 'navigation message,' which can be read by the user's GPS receiver. The navigation message includes orbit parameters (often called the 'broadcast ephemeris'), from which the receiver can compute satellite coordinates (X, Y, Z) . These are Cartesian coordinates in a geocentric system, known as WGS 84, which has its origin at the Earth's center of mass, Z-axis pointing toward the North Pole, X pointing toward the prime meridian (which crosses Greenwich), and Y at right angles to X and Z to form a right-handed orthogonal coordinate system. The algorithm that transforms the orbit parameters into WGS 84 satellite coordinates at any specified time is called the 'Ephemeris Algorithm' (e.g., Leick, 2004). For geodetic purposes, precise orbit information is available over the Internet from civilian organization such as the IGS in the Earth-fixed reference frame.

According to Kepler's laws of orbital motion, each orbit takes the approximate shape of an ellipse, with the Earth's center of mass at the focus of the ellipse (Figure 5). For a GPS orbit, the

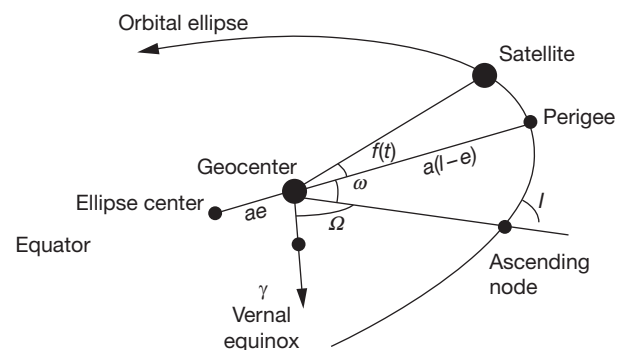


Figure 5 Diagram illustrating the Keplerian orbital elements: semimajor axis a , eccentricity e , inclination l , argument of perigee (closest approach) ω , right ascension of the ascending node Ω , and true anomaly f as a function of time t . The geocenter is the Earth's center of mass; hence, satellite geodesy can realize the physical origin of the terrestrial reference system. This diagram is exaggerated, as GPS orbits are almost circular.

eccentricity of the ellipse is so small (0.02) that it is almost circular. The semimajor axis (largest radius) of the ellipse is approximately 26 600 km, or approximately 4 Earth radii.

The six orbital planes rise over the equator at an inclination angle of 55° . The point at which they rise from the Southern to Northern Hemisphere across the equator is called the 'right ascension of the ascending node.' Since the orbital planes are evenly distributed, the angle between the six ascending nodes is 60° .

Each orbital plane nominally contains four satellites, which are generally not spaced evenly around the ellipse. Therefore, the angle of the satellite within its own orbital plane, the 'true anomaly,' is only approximately spaced by 90° . The true anomaly is measured from the point of closest approach to the Earth (the perigee). Instead of specifying the satellite's anomaly at every relevant time, it is equivalent to specify the time that the satellite had passed perigee and then compute the satellite's future position based on the known laws of motion of the satellite around an ellipse. Finally, the argument of perigee specifies the angle between the equator and perigee. Since the orbit is nearly circular, this orbital parameter is not well defined, and alternative parameterization schemes are often used.

Taken together (the eccentricity, semimajor axis, inclination, right ascension of the ascending node, time of perigee passing, and argument of perigee), these six parameters define the satellite orbit (according to the Keplerian model). These parameters are known as Keplerian elements. Given the Keplerian elements and the current time, it is possible to calculate the coordinates of the satellite.

However, GPS satellites do not move in perfect ellipses, so additional parameters are necessary. Nevertheless, GPS does use Kepler's laws to its advantage, and the orbits are described in the broadcast ephemeris by parameters that are Keplerian in appearance. Additional parameters must be added to account for non-Keplerian behavior. Even this set of parameters has to be updated by the control segment every hour for them to remain sufficiently valid.

Several consequences of the orbit design can be deduced from the previously mentioned orbital parameters and Kepler's laws of motion. First of all, the satellite speed is $\sim 4 \text{ km s}^{-1}$ relative to the Earth's center. All the GPS satellite orbits are prograde, which means the satellites move in the direction of the Earth's rotation. Therefore, the relative motion between the satellite and a user on the ground must be less than 4 km s^{-1} . Typical values around 1 km s^{-1} can be expected for the relative speed along the line of sight (range rate).

The second consequence is the phenomena of 'repeating ground tracks' every day. The orbital period is approximately $T = 11 \text{ h } 58 \text{ min}$; therefore, a GPS satellite completes two revolutions in $23 \text{ h } 56 \text{ min}$. This is intentional, as it equals one sidereal day, the time it takes for the Earth to rotate 360° . Therefore, every day (minus 4 min), the satellite appears over the same geographic location on the Earth's surface. The 'ground track' is the locus of points on the Earth's surface that is traced out by a line connecting the satellite to the center of the Earth. The ground track is said to repeat. From the user's point of view, the same satellite appears in the same direction in the sky every day minus 4 min. Likewise, the 'sky tracks' repeat.

So from the point of view of a ground user, the entire satellite geometry repeats every sidereal day. Consequently,

any errors correlated with satellite geometry will repeat from one day to the next. An example of an error tied to satellite geometry is 'multipath,' which is due to the antenna also sensing signals from the satellite that reflect and refract from nearby objects. In fact, it can be verified that, because of multipath, observation residuals do have a pattern that repeats every sidereal day. Therefore, such errors will not significantly affect the repeatability of coordinates estimated each day. However, the accuracy can be significantly worse than the apparent precision for this reason.

Another consequence of this is that the same subset of the 24 satellites will be observed every day by someone at a fixed geographic location. Generally, not all 24 satellites will be seen by a user at a fixed location. This is one reason why there needs to be a global distribution of receivers around the globe to be sure that every satellite is tracked sufficiently well.

The inclination angle of 55° also has consequences for the user. Note that a satellite with an inclination angle of 90° would orbit directly over the poles. Any other inclination angle would result in the satellite never passing over the poles. From the user's point of view, the satellite's sky track would never cross over the position of the celestial pole in the sky. In fact, there would be a 'hole' in the sky around the celestial pole where the satellite could never pass. For a satellite constellation with an inclination angle of 55° , there would therefore be a circle of radius at least 35° around the celestial pole, through which the sky tracks would never cross. This has a big effect on the satellite geometry as viewed from different latitudes. An observer at the pole would never see a GPS satellite rise above 55° elevation. Most of the satellites would hover close to the horizon. Therefore, vertical positioning is slightly degraded near the poles. An observer at the equator would see some of the satellites passing overhead but would tend to deviate away from points on the horizon directly to the north and south.

Due to a combination of the Earth's rotation and the fact that the GPS satellites are moving faster than the rotation of the Earth, the satellites actually appear to move approximately north-south or south-north to an observer at the equator, with very little east-west motion. Therefore, the closer the observer is to the equator, the better determined the north component of relative position becomes as compared with the east component. An observer at midlatitudes in the Northern Hemisphere would see satellites anywhere in the sky to the south, but there would be a large void toward the north. This has consequences for site selection, where a good view is desirable to the south, and the view to the north is less critical. For example, one might want to select a site in the Northern Hemisphere that is on a south-facing slope (and vice versa for an observer in the Southern Hemisphere).

3.11.2.3 Introducing High-Precision GPS

By measuring pseudoranges to at least four satellites with relatively low-cost equipment, GPS can readily provide users with a positioning accuracy of meters and a timing accuracy of $0.1 \mu\text{s}$. On the other hand, geodetic GPS positioning with an accuracy of a few millimeters requires a number of significant improvements to the technique described in the preceding text, which will be emphasized in this section. For example,

accurate positioning requires accurate knowledge of the GPS satellite positions and satellite clock offsets. For standard GPS positioning, this 'ephemeris' information is broadcast by the GPS satellites in the so-called navigation message; however, it is not sufficiently accurate for geodetic applications.

In addition to the three GPS segments listed earlier, one could informally include the 'service segment' consisting of civilian networks that provide the user segment with data and services to enhance positioning accuracy. This information can be transmitted to the user in a variety of ways, such as by the Internet, cell phone, and geostationary satellite. The part of this service segment that is relevant to geodetic positioning would be the International GNSS Service (IGS), an international collaboration of geodesists that provides high-accuracy data on satellite orbits and clocks. IGS also provides data from reference stations around the globe, at accurately known coordinates that account for plate tectonics and other geophysical movements such as earthquakes. Thus, the IGS enables users to position their receivers anywhere on the globe with an accuracy of millimeters in a consistent terrestrial reference frame. But this is only solves one of the many problems toward achieving geodetic precision.

In practice, high-precision GPS geodesy requires a minimum of five satellites in view, because it is essential to estimate parameters to model tropospheric refraction. At an absolute minimum, one zenith delay is estimated, which can be mapped to delay at any elevation angle using a 'mapping function' based on tropospheric models.

Geodetic applications require much more sophisticated GPS receivers that measure not only the pseudorange observable but also the so-called 'carrier phase' observable. The carrier phase observable is the difference between (1) the phase of the incoming carrier wave (upon which the codes are transmitted) and (2) the phase of a signal internally generated by the receiver, which is synchronized with the receiver clock. When multiplied by the ~ 20 cm wavelength of the carrier wave, the result is a biased distance to the satellite. Indeed, this is a type of pseudorange that is about 100 times more precise than the coded pseudoranges. The downside to the carrier phase observable is that in addition to the receiver clock bias, there is an additional bias of an unknown number of wavelengths. It is possible to resolve this bias exactly by the so-called 'ambiguity resolution' techniques. Ambiguity resolution is essential to achieve the highest possible precision for geodetic applications. Hence, in units of range, the observed carrier phase can be expressed as

$$\begin{aligned} \text{carrier_phase} = & (\text{reference_phase} - \text{signal_phase} + \text{integer}) \\ & \times \text{carrier_wavelength} \end{aligned} \quad [2]$$

Note that the signal phase is generated by the satellite clock and that the reference phase is generated by the receiver clock; hence, eqn [2] is just a very precise form of eqn [1] for the pseudorange, except that it has an integer-wavelength ambiguity. (In fact, this is why the sign of the phase difference was chosen by subtracting the incoming signal phase from the reference phase.) Therefore, the observable models for eqns [1] and [2] are very similar and relate to the theoretical difference between the reading of the receiver clock (time of reception) and the satellite clock (time of transmission), including clock biases.

This similarity of models has enabled the development of automatic signal processing algorithms to check the integrity of the data, such as the detection of data outliers and jumps in the integer ambiguity (the so-called cycle slips), which occur when the receiver loses lock on the signal, for example, due to a temporary obstruction between the ground antenna and the satellite. In fact, the pseudorange data can be used together with the carrier phase data to correct for the initial integer ambiguity (Blewitt, 1989) and for subsequent cycle slips (Blewitt, 1990).

For geodetic positioning, both pseudoranges and carrier phases are measured at two different frequencies (L1 at 19.0 cm wavelength and L2 at 24.4 cm), to provide a self-calibration of delay in the Earth's ionosphere. So in total, there are four observations that are fundamental to high-precision GPS geodesy: two pseudoranges and two carrier phases. This enables more algorithms to assure the integrity of the data and allows for monitoring of the ionosphere itself.

Another requirement for geodetic positioning is the use of highly specialized stochastic multiparameter estimation software by modeling the carrier phase data, including modeling of the satellite-station geometry, Earth's atmosphere, solid Earth tides, Earth's rotation, antenna effects, circular polarization effects (phase windup), and relativistic effects (both special and general). In addition, the software must be capable of detecting and correcting integer offsets in the carrier phase observables (cycle slips) and must be capable of resolving the integer ambiguity in the initial phase measurements.

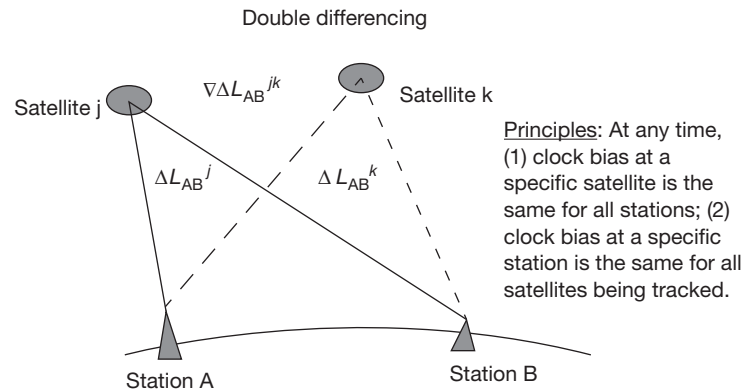
In summary, therefore, geodetic GPS requires

- geodetic-class GPS receivers capable of acquiring dual-frequency carrier phase data;
- geodetic-class satellite orbit and clock information, which is available from the IGS;
- simultaneous observations to a minimum of five satellites;
- specialized postprocessing software (not on the receiver itself) that embodies high-accuracy observable models, carrier phase data processing algorithms, and simultaneous parameter estimation.

The quality of the IGS orbit and clock data depends on their latency, so generally, there is a trade-off between latency and accuracy. Currently, the ultrarapid IGS product is actually a prediction from 3 to 9 h ago. Even though there are atomic clocks on board the GPS satellites, the clock time is much more difficult to predict than the satellite orbits. In the case that sufficiently accurate clock data are not yet available, it is nevertheless possible to produce geodetic-class solutions for relative positions between ground stations. This is achieved either by (1) solving for satellite clock biases at every epoch as part of the positioning solution or equivalently by (2) differencing data between ground stations to cancel out the clock bias. Furthermore, data can be differenced again ('double difference') between satellites to cancel out the receiver clock bias rather than estimate it as a parameter (Figure 6).

In practice, the following different approaches to estimating positions all give results that are of geodetic quality (with errors measured in millimeters) and typically agree very well:

- Precise point positioning (PPP) of single stations using precise orbit and clock data.



At each epoch, difference the single difference data between satellites:

$$\nabla\Delta L_{AB}^{jk} = \Delta L_{AB}^j - \Delta L_{AB}^k$$

Figure 6 Diagram illustrating double differencing of GPS data. The idea is to differentiate away the satellite and station clock biases. Double differencing is equivalent to estimating the clock biases explicitly when processing undifferenced data.

- Relative positioning of networks by clock estimation, using precise orbit data.
- Relative positioning of networks by double-difference data (Figure 6), using precise orbit data.

All of these three methods are in common use today for geophysical research purposes. In each case, dual-frequency pseudorange and carrier phase data types are used.

3.11.2.4 GPS Observable Modeling

This section describes how GPS observables are typically modeled by geodetic-quality software packages. First, however, a few more specific details on the GPS signals are required. The signals from a GPS satellite are fundamentally driven by an atomic clock precisely at frequency 10.23 MHz. Two sinusoidal carrier signals are generated from this signal by multiplying the frequency by 154 for the L1 channel (frequency = 1575.42 MHz; wavelength = 19.0 cm) and 120 for the L2 channel (frequency = 1227.60 MHz; wavelength = 24.4 cm). Information is encoded in the form of binary bits on the carrier signals by a process known as phase modulation. The binary digits 0 and 1 are actually represented by multiplying the electrical signals by either +1 or -1.

For purposes of observable modeling, here, the observables (all in units of meters) will be called L1 and L2 for the two types of carrier phase and P1 and P2 for the two types of pseudorange. The actual observable types are numerous due to different methods of correlating the signals; however, the fundamental observation equations can be written in the same generic way, with the exception that there is generally a bias associated with each observable types, including instrumental bias and, in the case of the carrier phase, an integer wavelength bias. (For some older signal-squaring receivers, the bias is a half-integer wavelength.) Here, it is simply assumed that such biases are not problematic, which is typically the case, and so the interobservable biases are not explicitly modeled.

Taking eqns [1] and [2], the generic (pseudorange or carrier phase) GPS observation P_j^i at receiver j (subscript, on the ground) from satellite i (superscript, up in space) can be modeled:

$$P_j^i = c(T_j - \bar{T}^i) + B_j^i \quad [3]$$

Since special relativity and general relativity prove to be important in the model, care must be taken to define each term with respect to a reference frame. Thus, T_j is the time according to the receiver clock coincident with signal reception (used as the time tag, recorded with the observation), \bar{T}^i is the time according to the satellite clock coincident with signal transmission (which imprints its signature on the signal, hence the bar, which denotes time local to the satellite), B_j^i is a frame-invariant bias associated with this type of observation, and c is the frame-invariant speed of light in a vacuum. In addition, this observation is recorded at an epoch with time tag T_j (the same for all satellites observed at that epoch).

The clock difference can be rewritten as the sum of four time differences:

$$P_j^i = c\left\{(T_j - t_j) + (t_j - t^i) + (t^i - \bar{t}^i) + (\bar{t}^i - \bar{T}^i)\right\} + B_j^i \quad [4]$$

where t_j is the coordinate time at the receiver, t^i is the coordinate time at the satellite, and \bar{t}^i is the proper time at the satellite (the time kept by a perfect clock on board the satellite). 'Coordinate time' simply means the timescale that is actually used to compute the models. It is convenient to take coordinate time in the 'local Earth' frame (that of a perfect clock on the geoid) (Ashby and Allan, 1984). Appropriate timescales for this purpose include Terrestrial Dynamic Time (TDT) and International Atomic Time (TIA), but for the discussion here, it is convenient to choose GPS time. The important thing to keep in mind (to cut through the confusion of all these conventions) is that all these timescales ideally run at the same rate as UTC, with the unit of time being the SI second (Kaplan, 1981), and so all these scales only differ by conventional constant offsets (and leap seconds).

The four time-difference terms found in eqn [4] can be written as follows. First, the difference in receiver clock time and coordinate time is simply the receiver clock bias, which we will model as an independent parameter τ_j at every epoch (at every value of T_j):

$$(T_j - t_j) = \tau_j \quad [5]$$

The clock bias includes the sum of a clock error (with respect to proper time) plus a minor relativistic bias due to the geodetic location of the receiver clock.

The second term is the difference between coordinate time at the receiver and satellite, the so-called light-time equation (here expressed as a range):

$$\begin{aligned} c(t_j - t^i) &= r_j^i + \sum_{\text{prop}} \Delta r_{\text{prop}_j}^i \\ &= |\mathbf{r}_j(t_j) - \mathbf{r}^i(t^i)| + \Delta r_{\text{GR}_j}^i + \Delta r_{\text{ion}_j}^i + \Delta r_{\text{trop}_j}^i \\ &\quad + \Delta r_{\text{pcvj}_j}^i + \Delta r_{\text{circ}_j}^i + \dots \end{aligned} \quad [6]$$

where r_j^i is the Euclidean distance between the satellite and receiver and $\Delta r_{\text{prop}_j}^i$ represent various propagation delays, which are a function of satellite-station geometry, arising from space-time curvature (general relativity); ionosphere, troposphere, and antenna phase center variations; circular polarization effects; and other propagation terms as necessary. In eqn [6], \mathbf{r}_j is the geocentric receiver position at the time of reception and \mathbf{r}^i is the geocentric satellite position at the time of transmission. The reference frame for the light-time equation is taken to be J2000, the conventional Earth-centered inertial (ECI) frame (so the axes do not corotate with the Earth), because the speed of light is a constant in all directions in an inertial frame. In addition, the ECI frame is most convenient for integrating the satellite equations of motion, if the goal is to estimate satellite orbits. However, it can be more convenient to solve the light-time equation in a rotating, Earth-centered, Earth-fixed (ECEF) reference frame, given that satellite orbit positions and velocities are typically distributed in the ECEF frame. In this case, the equation would also need to account for the Sagnac effect (e.g., Ashby, 2004), which accounts for the effect of the Earth's rotation on light propagation when viewed in the ECEF frame. A simple way to handle this is to consider the ECEF and ECI frames as being instantaneously aligned at reception time. Thus, all that is required is to compute the satellite velocity in the ECI frame by adding the velocity due to the Earth's rotation at the satellite to the ECEF velocity and then compute the ECI position of the satellite at transmit time using this ECI velocity. Thus, the Sagnac effect can be considered simply as a correction for the Earth's rotation.

The general relativistic delay can be computed as

$$\Delta r_{\text{GR}_j}^i = \frac{2GM_{\oplus}}{c^2} \ln \frac{r_j + r^i + r_j^i}{r_j + r^i - r_j^i} \quad [7]$$

where GM_{\oplus} is the Earth's gravitational constant and, in general, $r \equiv |\mathbf{r}|$. This is sometimes called the Shapiro delay after Shapiro (1964) and is typically at the 10 mm level for signals from satellites in medium Earth orbit. It accounts for the distance traveled, being longer than the Euclidean distance, caused by space-time curvature in the Earth's gravitational field. Equation [7] is a sufficiently good approximation, derived by integrating the effect of the Earth's gravitational potential along a

straight light path; so the term 'space-time curvature' should not be confused with gravitational bending of the direction of light, which is negligible. Rather, the curvature can be thought of primarily as the 'stretching' of space along the direction of travel.

Antenna effects such as phase center variation Δr_{pcvj}^i [Schupler et al., 1994] and circular polarization $\Delta r_{\text{circ}_j}^i$ ('phase windup') (Wu et al., 1993) are examples of important effects that have been researched and applied to improve positioning accuracy, but as nongeophysical effects, they are beyond the scope of this text. Antenna calibrations for both the GPS satellite and station antennas are available from the IGS and should be applied (Schmid et al., 2005).

Ionospheric delay can be adequately modeled as being inversely proportional to the squared frequency f of the carrier wave:

$$\Delta r_{\text{ion}_j}^i(f) = \pm k \frac{\text{TEC}_j^i}{f^2} \quad [8]$$

where the positive sign is taken for pseudoranges and the negative sign for carrier phase observations. The term TEC refers to 'total electron content,' which is excited by solar radiation and so is highly variable through the day and is sensitive to geographic location. The constant k can be derived from the theory of electromagnetic (EM) wave propagation in plasmas. Delays at GPS frequencies can be as large as 100 m near the equator, peaking around 2 pm local time, and can be as small as centimeters at midlatitudes between midnight and dawn. In contrast, higher-order terms are of the order of millimeters and are typically ignored, although including them in the model is one of many themes of current research (Kedar et al., 2003). An appropriate linear combination of observations eliminates the frequency-squared term exactly, leaving all nondispersive terms in the model unchanged. In fact, the 'ionosphere-free' combination of carrier phases can be so defined (and similarly for the pseudoranges):

$$\begin{aligned} \text{LC} &= \frac{f_1^2 L1 - f_2^2 L2}{(f_1^2 - f_2^2)} \\ &\cong 2.546L1 - 1.546L2 \end{aligned} \quad [9]$$

Hence, k and TEC are not explicitly needed to compute the ionosphere-free data. The coefficients in the preceding text can be computed exactly by substituting $f_1 = 154$ and $f_2 = 120$, owing to the properties of the GPS signals described at the beginning of this section. As an aside, if the ionosphere is the geophysical scientific target of interest, then differencing the observations at two different frequencies results in a 'geometry-free' observation from which TEC can be estimated:

$$\begin{aligned} PI &= P1 - P2 \\ &= k\text{TEC} \left(\frac{1}{f_1^2} - \frac{1}{f_2^2} \right) + \text{bias} \end{aligned} \quad [10]$$

Using GPS stations located around the globe, this method is now routinely used to map ionospheric TEC. A side benefit of this method is the estimation of the interchannel bias between observables at L1 and L2 frequency, which can be monitored for long-term variability and used as input to ambiguity resolution algorithms.

The tropospheric delay (a fraction of which actually occurs in the stratosphere) is almost entirely nondispersive

(independent of frequency) at GPS L-band frequencies and so must be handled in a different way. Whereas it is possible in principle to model tropospheric delay based on ground-based meteorologic observations, in practice, this has not proven to be sufficiently accurate. The key to successful tropospheric modeling is the estimation of the delay at zenith, by accurately modeling the relationship between zenith delay Z and delay at lower elevations ε , for example,

$$\Delta r_{\text{trop}_j}^i = \frac{Z_j}{\sin \varepsilon_j^i} \quad [11]$$

where the inverse sign of elevation angle is the simplest example of a 'mapping function,' which can be derived by assuming a horizontally layered troposphere over a flat Earth. This model breaks down rapidly for $\varepsilon < 20^\circ$. More accurate modeling (Truehaft and Lanyi, 1987) requires modifying the mapping function to account for Earth curvature and partitioning the delay into a so-called dry and wet components, which have different characteristic scale heights (~ 10 km and ~ 2 km, respectively):

$$\begin{aligned} \Delta r_{\text{trop}_j}^i &= \Delta r_{\text{dry}_j}^i + \Delta r_{\text{wet}_j}^i \\ &= Z_{\text{dry}} F_{\text{dry}}(\varepsilon_j^i) + Z_{\text{wet}} F_{\text{wet}}(\varepsilon_j^i) \end{aligned} \quad [12]$$

Due to the inherent weakness in the determination of height with both GPS and VLBI, accurate modeling of mapping functions has always been and remains an active area of research. The wet delay is caused by the interaction of the EM wave with the static dipole of molecular water. The dry delay is due to the dynamic dipole induced by the EM wave on all component molecules in the atmosphere, including a (small) contribution from water (and so 'dry' is just a conventional, perhaps, misleading term). Typical values for the dry and wet delay are 2.1 and 0.1 m, respectively, to within ~ 10 cm.

The dry component can be adequately modeled as a function of hydrostatic pressure at the altitude of the receiver. Nominal values can be computed in the absence of meteorologic data by assuming a nominal surface pressure at sea level and then subtracting a correction for altitude, assuming that pressure decays exponentially with altitude. The wet component is typically assumed to have a nominal value of zero, and Z_{wet} is then estimated from the GPS data along with the positioning solution. Note that in this case, the estimated value of Z_{wet} would absorb most (but not all) of the obvious inadequacies of the nominal model for Z_{dry} . Whereas this is currently the standard method in high-precision GPS geodesy, the limitations of this approach are an active area of research (Tregoning and Herring, 2006).

The tropospheric delay model is important not only for solving for geodetic position but also for the study of the troposphere itself. For this application, estimates of troposphere delay can be converted into precipitable water vapor in the atmosphere, which can then be used as input for weather forecasting and climate modeling. For this application, surface meteorologic data are essential to more accurately partition the dry and wet components of delay (Bevis et al., 1992).

Now, returning to the light-time equation, even if we had perfect propagation models, the light-time equation needs to be solved iteratively rather than simply computed, because at first, we do not have a nominal value for t^i , the coordinate time of signal transmission. The procedure is as follows:

- Starting with the observation time tag T_j , use eqn [5] and a nominal value for the receiver clock bias τ_j (which may be zero or a preliminary estimate) to compute the coordinate time of signal reception t_j . Note that the assumed clock bias affects the subsequent computation of geometric range, indicating the need for iterative estimation. (This problem can be more conveniently addressed by accounting for the range rate in the partial derivative with respect to the receiver clock parameter.)
- Given a modeled station position \mathbf{r}_j at time t_j , and an interpolated table of modeled satellite positions \mathbf{r}^i as a function of coordinate time t^i , iteratively compute the coordinate time of transmission using

$$ct^i[n+1] = ct^i[n] + \frac{ct_j - ct^i[n] - r_j^i[n] - \sum_{\text{prop}} \Delta r_{\text{prop}_j}^i[n]}{1 - \hat{\mathbf{r}}^i[n] \cdot \hat{\mathbf{r}}_j^i[n]/c} \quad [13]$$

where $\hat{\mathbf{r}}^i = \mathbf{r}_j^i / r_j^i$ are the direction cosines to the receiver from the satellite. It is to be understood that at the n th iteration, for example, the satellite position \mathbf{r}^i and ECI velocity $\dot{\mathbf{r}}^i$ are both interpolated to time $t^i[n]$. By virtue of this equation converging very quickly, it is sufficient to initialize the transmission time to the reception time $t^i[0] = t_j$.

Being in the ECI frame (J2000), the receiver position must account for the Earth's rotation and geophysical movements of the Earth's surface:

$$\mathbf{r}_j(t_j) = \text{PNUXY} \left[\mathbf{x}_{0j} + \sum_k \Delta \mathbf{x}_{kj}(t_j) \right] \quad [14]$$

Here, **PNUXY** is the multiple of 3×3 rotation matrices that account (respectively) for precession, nutation, rate of rotation, and polar motion (in two directions). The bracketed term represents the receiver position in the (corotating) conventional Earth-fixed terrestrial reference frame known as ITRF. Conventional station position \mathbf{x}_{0j} is specified by station coordinates in ITRF at some conventional epoch, and $\Delta \mathbf{x}_{kj}(t_j)$ represents the displacement from the epoch position due to geophysical process k , for example, accounting for the effects of plate tectonics, solid Earth tides, etc. Equation [14] together with [6] forms the fundamental basis of using GPS as a geophysical tool, and this will be explored later.

Returning now to the original observation eqn [4], the third term is the difference between coordinate time and proper time at the satellite. According to special relativity, GPS satellite clocks run slow relative to an observer on the Earth's surface due to relative motion. In contrast, general relativity predicts that the satellite clocks will appear to run faster when observed from the Earth's surface due to the photons gaining energy (gravitational blue shift) as they fall into a gravitational well. These two effects do not entirely cancel. With appropriate foresight in the design of GPS, the satellite clocks operate at a slightly lower frequency than 10.23 MHz to account for both special relativity and general relativity, so that their frequency would be 10.23 MHz (on average) as viewed on the Earth's surface. The residual relativistic term can be computed from

$$(t^i - \bar{t}^i) = 2\mathbf{r}^i(t^i) \cdot \dot{\mathbf{r}}^i(t^i) / c^2 \quad [15]$$

It is inconsequential as to whether eqn [15] is computed in the ECI or ECEF frame. This result assumes an elliptical orbit

about a point (or spherically layered) mass and assumes that additional relativistic effects are negligible. The expected accuracy is at the level of 10^{-12} , comparable with the level of stability of the satellite atomic clocks.

The fourth term is the difference between proper time and clock time at the satellite, which is simply the negative error in the satellite clock:

$$\left(\bar{t}^i - \bar{T}^i\right) = -\tau^i \quad [16]$$

Unlike errors in the station clock, errors in the satellite clock do not affect the model of geometric range (in the light-time equation) and so are not required in advance to compute that part of the model. However, they do affect the observable itself, and so not accounting for satellite clock error would result in an error in estimated receiver position. Despite the satellite clocks being atomic, they are not sufficiently stable to be predicted forward in time for geodetic applications (though this is the method for standard positioning with GPS). Therefore, this term is estimated independently at every epoch as part of the positioning solution (or alternatively, observations equations can be differenced between pairs of observing receivers to eliminate this parameter). As a consequence, geodetic-quality PPP of individual stations in real time presents a challenge that is the topic of current research.

Finally, each observation type has an associated bias. Typically, receivers are designed so that these biases either should be calibrated or are stable in time. Like the case for the satellite clock error, these biases have no effect on the computed geometric range and so do not need to be known in advance; however, they are present in the observations themselves and so can affect positioning accuracy unless they are absorbed by parameters in the least-squares solution. It turns out for the most part that biases between observable types can be ignored for purposes of positioning, because they can be absorbed into the station or satellite clock bias parameters as part of the least-squares positioning solution. For purposes of accurate timing, however, special considerations are required to calibrate such biases. Some of the inter-observable biases are monitored by major GPS analysis centers and made routinely available if needed.

The most important bias to consider for geodetic applications is the carrier phase bias, for which its double difference has an integer ambiguity (Blewitt, 1989). The carrier phase bias is not predictable from models and can vary by integer jumps occasionally (Blewitt, 1990). For an initial solution, the carrier phase biases can be nominally assumed to be zero (because they do not affect the light-time equation) and then estimated as real-valued parameters. If the real-valued carrier phase bias parameters are sufficiently precise, then their double differences can be resolved to their correct integer values. The solution can then be computed again by holding these integer values fixed, or more efficiently, the change to the solution can be computed using least-squares adjustment theory.

For undifferenced data processing, such as PPP, ambiguity resolution presents a conundrum. A solution to this problem lies in the stability of undifferenced phase biases. It turns out that the double difference in the estimates of the phase biases can be resolved to integer numbers of cycles (Blewitt, 1989). In the case of PPP with a single receiver (Zumberge et al., 1997),

we also need estimates of biases from at least one other station with the same satellites in view. A successful method now in common use, which was proposed and demonstrated by Bertiger et al. (2010), is known as the wide-lane and phase bias (WLPB) method. The WLPB method estimates biases for the IGS network during the GPS orbit estimation procedure. These phase bias estimates are then made available to the single-receiver user along with the GPS orbit and clock parameters. Thus, the user can perform ambiguity resolution when PPP with a single receiver.

In summary, this has been a key section, in that the light eqn [6] represents the heart of GPS observable modeling and a very specific component given by eqn [14] is the source of all geophysical applications that relate to precise positioning.

3.11.2.5 Data Processing Software

Geodetic GPS data processing as implemented by research software packages can typically be generalized as a modular scheme (Figure 7). In this processing model, the input is raw data from GPS receivers, and the processing stops with the production of a set of station coordinates. Before discussing data processing in detail, it should be noted that the data processing does not stop with the initial production of station coordinates, but rather this is the first step toward time series analysis, velocity estimation, and kinematic analysis, all leading to dynamic analysis and geophysical interpretation. It is convenient to separate the actual processing of GPS data shown in the preceding text from the subsequent kinematic analysis, though for some geophysical applications (e.g., ocean tidal loading), this division is not correct, and geophysical parameters must be estimated directly in the solution.

Several software packages have been developed since the 1980s that are capable of delivering high-precision geodetic estimates over long baselines. These days, the processing of GPS data by these software packages is, to a large degree, automatic, or at least a 'black-box' approach is common. The black box can of course be tampered with for purposes of research into GPS methodology, but one big advantage of automation is reproducibility and consistency of results produced in an objective way.

Geodetic data processing software is a result of intensive geodetic research, mainly by universities and government research laboratories. Typical features of such software include

- orbit integration with appropriate force models;
- accurate observation model (Earth model, media delay, etc.) with rigorous treatment of celestial and terrestrial reference systems;
- reliable data editing (cycle slips and outliers);
- estimation of all coordinates, orbits, tropospheric bias, receiver clock bias, polar motion, and Earth spin rate;
- ambiguity resolution algorithms applicable to long baselines;
- estimation of reference frame transformation parameters and kinematic modeling of station positions to account for plate tectonics and coseismic displacements.

The typical quality of geodetic results from processing 24 h of data can be summarized as follows (IGS, <http://igsceb.jpl.nasa.gov>):

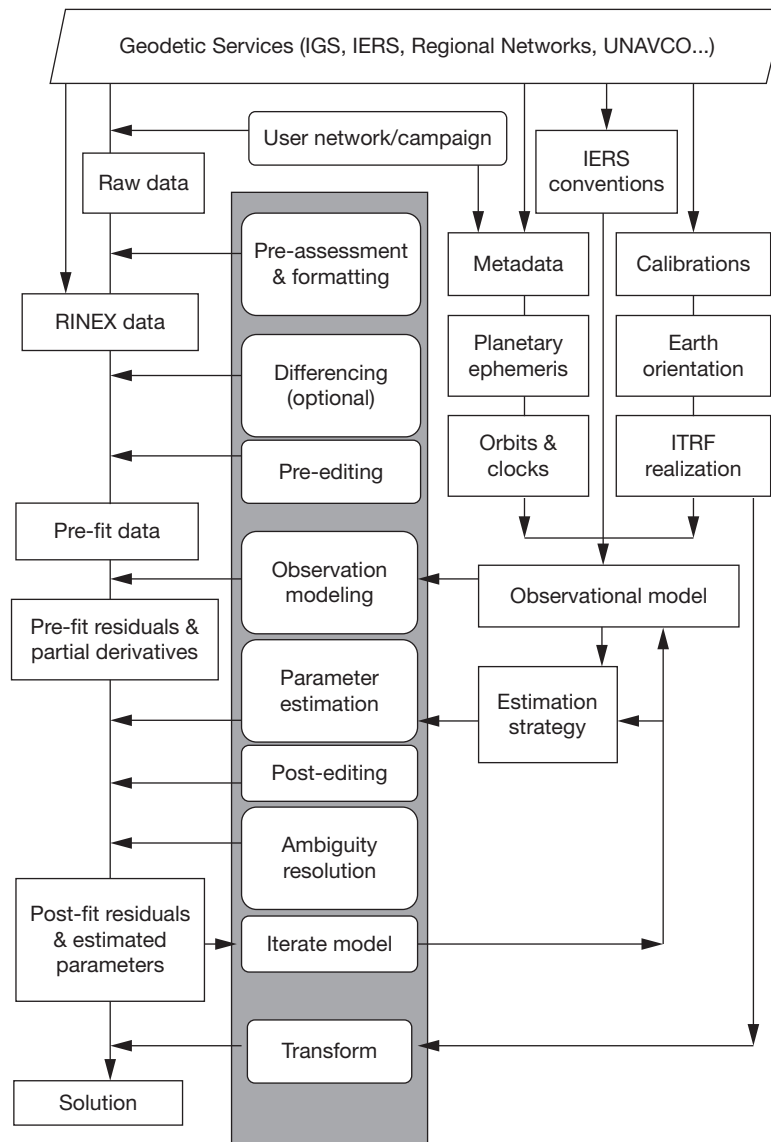


Figure 7 Generic modular scheme for geodetic GPS data processing.

- Relative positioning at the level of few parts per billion of baseline length
- Geocentric (global) positioning to ~ 6 mm vertical and ~ 3 mm horizontal in the ITRF
- Tropospheric delay estimated to ~ 4 mm
- GPS orbits determined to ~ 25 mm
- Earth pole position determined to ~ 2 mm
- Clock synchronization (relative bias estimation) to < 0.1 ns
- Ionospheric TEC maps to < 10 TEC units

Two features of commercial software are often conspicuously absent from more advanced packages: (1) Sometimes, double differencing is not implemented, but instead, undifferenced data are processed, and clock biases are estimated; (2) network adjustment using baseline solutions is unnecessary, since advanced packages do a rigorous, one-step, simultaneous adjustment of station coordinates directly from all available GPS observations.

Some precise software packages incorporate a Kalman filter (or an equivalent formalism) (Bierman, 1977; Herring et al., 1990; Lichten and Border, 1987). This allows for certain selected parameters to vary in time, according to a statistical ('stochastic') model. Typically, this is used for the tropospheric bias, which can vary as a random walk in time (Tralli and Lichten, 1990). A filter can also be used to estimate clock biases, where 'white noise' estimation of clock bias approaches the theoretical equivalent of double differencing.

Although many more packages have been developed, there are three ultrahigh-precision software packages, which are widely used around the world by researchers and are commonly referenced in the scientific literature:

- Bernese software, by Astronomical Institute, University of Bern, Switzerland (Rothacher et al., 1990);
- GAMIT-GLOBK software, by Massachusetts Institute of Technology, the United States (King and Bock, 2005);

- GIPSY-OASIS II software, by JPL, California Institute of Technology, the United States (Webb and Zumbege, 1993).

There are several other packages, but they tend to be limited to the institutions that wrote them. It should be noted that, unlike commercial software packages, the use of the previously mentioned software can require a considerable investment in time to understand the software and how best to use it under various circumstances. Expert training is essential.

3.11.2.6 Real-Time GPS and Accuracy Versus Latency

The most accurate GPS geodetic solutions result from a simultaneous estimation for satellite orbit and clock parameters, Earth rotation parameters, and station coordinates. On the other hand, solutions that very closely approximate those from simultaneous estimation are possible in a two-step process, where an analysis center first computes the satellite orbit and clock parameters and Earth rotation parameters and then distributes these to users who simply solve for their own station coordinates (along with the station clock, tropospheric delay, and carrier phase biases). This is basically the model used by IGS and its analysis centers to serve its users.

One consequence of the two-step model is that there is a delay for the user, who must wait until the orbit parameters become available. In the extreme case of real-time positioning, the two-step model becomes challenging to implement accurately. In this case, the orbit positions must be predicted ahead in time, and the satellite clocks must be handled in real time, either by the user differencing data or by the analysis center providing real-time estimates of the satellite clock biases.

In this section, we consider the effect of latency on accuracy and precision of point positioning for the user with one of the best software packages available. We also consider the effect of positioning interval, for example, whether the position represents a 24 h average or a new position every data epoch, which could be every 5 min, every 1 s, or even shorter intervals. Positioning at every data epoch is sometimes called 'kinematic positioning,' which is somewhat of a misnomer, as positions are directly estimated rather than kinematic parameters such as velocity (which can be subsequently inferred from the position time series). Nevertheless, we use the term 'kinematic positioning' because it has become a *de facto* standard.

The most accurate 'final' orbits and clocks are available with 12–18 day latency (some as low as 5 days). These allow the user to perform daily PPP in the ITRF to a precision of ~2 mm horizontal and ~6 mm vertical using 24 h RINEX files. For kinematic positioning, the precision degrades to ~7 mm horizontal and ~20 mm vertical, as measured by RMS scatter over a day. However, the RMS precision can be much better than this over shorter time windows, so it is possible to track very accurately the variations in position caused by seismological waves. When using the term 'precision,' therefore, one must be careful to consider the time window relevant to the problem at hand.

GPS analysis centers also produce the so-called rapid orbits with 1–2 day latency. These products are almost as good as final orbits but can differ to the extent that quality control may

not be as effective at shorter latency. But as a consequence, positioning precision using rapid orbits is of similar quality to that using final orbits.

Pushing to lower latencies, GPS analysis centers also produce the so-called ultrarapid orbits with several-hour latency (some as low as 1–2 h latency). These tend to be based on the analysis of hourly RINEX files that have been concatenated over the last day or so. Ultrarapid orbits are useful for low-latency kinematic positioning problems, such as measuring the permanent displacement of stations following a large earthquake, and for rapidly inferring earthquake rupture parameters. Kinematic positioning using ultrarapid orbits is generally only slightly worse than using rapid orbits, at the 10 mm level horizontal and 30 mm level vertical. However, solutions can suffer because of several effects: (1) quality control becomes more difficult at lower latency; (2) toward the end of the ultrarapid orbit (closer to real time), the solution is based on data from the past, but not from the future, and so are degraded; (3) moreover, toward the end of the ultrarapid orbit, it becomes more difficult to detect and correct for the effect of cycle slips and to resolve integer ambiguities. As a consequence, the quality of positioning using ultrarapid orbits and clocks can be quite good but can also be sporadically poor in a rather unpredictable way.

Finally, at the extreme of real-time point positioning, it is sufficient to predict the future position of the ultrarapid orbits. However, the satellite clocks cannot be predicted accurately, and the issue of quality control becomes paramount. Moreover, the user is faced with the problem of having very poor initial estimates of carrier phase biases whenever new satellites come into view or whenever a cycle slip is detected. Carrier phase bias resets can cause systematic deviations of kinematic positions that do not reflect the actual motion of the station. Current real-time position precision is typically better than one decimeter but can be better or worse depending on the multipath and sky-view environment of the both the user's station and the stations used to determine the satellite clocks. Needless to say, improving real-time positioning is an emerging area of intense research.

3.11.3 Global and Regional Measurement of Geophysical Processes

3.11.3.1 Introduction

Geodesy is the science of the shape of the Earth, its gravitational field, and orientation in space and is therefore intrinsically connected to geophysics (Lambeck, 1988; Torge, 2001). Indeed, space geodetic techniques, such as GPS, can be used to observe the Earth and hence probe geodynamic processes on a global scale (Figure 8). GPS contributes to geophysics through comparing the observed and modeled motion of the Earth's surface. Since the observed motion of the Earth's surface will represent the sum of the various effects, it is clear that geophysics must be modeled as a whole, even when investigating a specific problem. This creates a rich area of interdisciplinary research.

As the precision and coverage of GPS stations have improved over the last two decades, the depth and breadth of GPS geodesy's application to geodynamics have increased

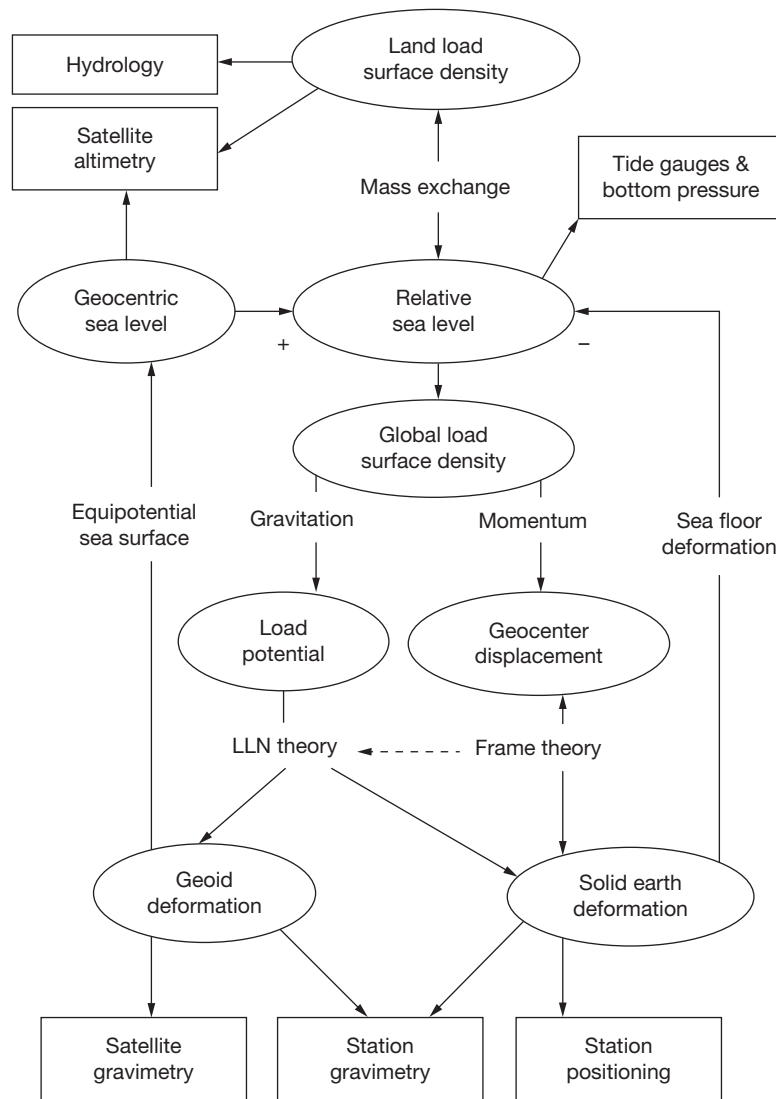


Figure 8 Schematic model of surface mass loading that incorporates self-consistency of the reference frame, loading dynamics, and passive ocean response. Closed-form inversion solutions have been demonstrated (Blewitt and Clarke, 2003; Gross et al., 2004). Note that everything is a function of time, so 'continental water' in its most general sense would include the entire past history of ice sheets responsible for postglacial rebound. (Arrows indicate the direction toward the computation of measurement models, phenomena are in round boxes, measurements are in rectangles, and physical principles label the arrows.)

correspondingly. It has now matured to the point that it is viewed as an important and often primary tool for understanding the mechanics of Earth processes.

On the other hand, geophysical models are essential to GPS geodesy; as such, models are embedded in the reference systems we use to define high-accuracy positions. For example, if the reference system did not account for the tidal deformation of the solid Earth, the coordinates of some stations could vary as much as ~ 10 cm in the time frame of several hours. Therefore, reference systems to enable high-accuracy geodetic positioning have developed in parallel with progress in geodynamics, which in turn depends on geodetic positioning. Thus, this interdependent relationship between geodesy and geophysics is inextricable.

Table 3 shows examples of the various geophysical processes that affect space geodetic observables and thus are

subject to investigation using space geodesy. Most of the applications assume the ability to track the position of geodetic stations with sub-centimeter precision, but other possibilities include the determination of the Earth's polar motion and rate of rotation, low-degree gravitational field coefficients, and atmospheric delay in the troposphere and ionosphere. For example, global climate change not only could affect both the shape and gravitational field through mass redistribution (e.g., melting polar ice caps) but also could affect large-scale tropospheric delay.

In this section, the focus will be on providing examples of geodetic applications across the spatiotemporal spectrum, ranging from coseismic rupture and seismic waves to plate rotations.

The subsequent section will then focus on how geodesy can be used to address large-scale loading problems.

Table 3 Geophysical processes that affect geodetic observations as a function of spatial and temporal scale

Scale	Temporal				
	10^{-2} – 10^3 s	10^0 – 10^1 h	10^0 – 10^2 day	10^0 – 10^2 year	10^2 – 10^6 year
10^0 – 10^1 km	Coseismic rupture Volcanism	Creep events Volcanism	Afterslip Poroelastic relaxation Dike injection	Viscoelastic relaxation Interseismic strain	Earthquake cycle
10^1 – 10^2 km	M 6–7.5 seismic strain release Tropospheric moisture	Storm-surge loading Tsunami loading Tropospheric moisture	Rifting events Aquifer deformation Poroelastic relaxation Lower crustal magmatism Lake loading Snow loading	Viscoelastic relaxation Block rotation Strain partition Mountain growth Glacial loading Sedimentary loading	Fault activation and evolution Mountain range building Denudation Regional topography Sedimentary loading
10^2 – 10^3 km	M 7.5–9 seismic strain release Traveling ionospheric disturbances Seismic waves	Coastal ocean loading	Atmospheric loading Regional hydrologic loading	Mantle–crust coupling Ice-sheet loading	Plateau rise Mountain range building Glacial cycle
10^3 – 10^4 km	M 9+ seismic strain release Seismic waves Free oscillations	Earth tides Tidal loading	Seasonal fluid transport Ocean bottom pressure	Core–mantle coupling Climate change Solar cycle	Plate rotations Mantle flow Continental evolution

3.11.3.2 Estimation of Station Velocity

All of the following examples use a time series of discrete station positions (whether they be relative station positions or with respect to the reference frame origin). For many applications, it is convenient to first fit a 3-D station velocity to each time series. If the velocity is intended to represent the secular motion of a station but the time series spans less than ~ 4.5 years, then it is important to simultaneously fit an empirical seasonal signal (Blewitt and Lavallée, 2002). The simplest seasonal model would fit amplitudes for an annual sine and cosine wave. In some locations, the semiannual signal may also be important, for example,

$$\begin{aligned} \mathbf{x}_i(t_j) = & \mathbf{x}_{i0} + \dot{\mathbf{x}}_i(t_j - t_0) + \mathbf{a}_{1i}^C \cos(2\pi t_j) + \mathbf{a}_{1i}^S \sin(2\pi t_j) \\ & + \mathbf{a}_{2i}^C \cos(\pi t_j) + \mathbf{a}_{2i}^S \sin(\pi t_j) + \mathbf{v}_{ij} \end{aligned} \quad [17]$$

where $\mathbf{x}_i(t_j)$ is the observed vector position of station i at epoch t_j (in Julian years); t_0 is an arbitrary user-specified time to define the modeled epoch position \mathbf{x}_{i0} ; $\dot{\mathbf{x}}_i$ is the station velocity (independent of the choice of t_0); the harmonic vector amplitude \mathbf{a}_{2i}^C , for example, indicates the cosine amplitude of frequency two cycles per year at station i ; and \mathbf{v}_{ij} represents the vector error. When using geocentric Cartesian coordinates, it is especially important to use a full 3×3 weight matrix in the inversion, because of the large difference (\sim factor of 3) in the magnitude of formal error in the vertical direction.

If the geophysical signals under investigation are seasonal in nature, then of course, the harmonic amplitudes are interesting in their own right, and the velocity term may be considered the ‘nuisance parameter.’ It should be always kept in mind that the parameter estimates will absorb the sum of all relevant geophysical processes and errors that affect the specified data set. Seasonal systematic errors are particularly difficult to quantify. In the case of simultaneous geophysical processes, it is

often the case that the larger-scale processes (e.g., global-scale plate tectonics) can be characterized first and used as a calibration or as boundary conditions for a smaller-scale study (e.g., plate boundary deformation).

For some applications, it may be sufficient to study the postfit residual time series (i.e., estimates of \mathbf{v}_{ij}). However, caution is warranted if the form of the signal under investigation significantly is likely to correlate with the velocity or harmonic amplitude parameters. If the exact form of the signal is known (e.g., a step function in the case of a coseismic displacement field), then it is always better to augment the model in the preceding text and estimate the extra parameters simultaneously with the previously mentioned base set of parameters. On the other hand, if the exact form is not known but the signal is assumed to start with an event at a given time T , then a reasonable approach is to estimate the base parameters using only data prior to time T and then form the residuals time series for all data using this model.

Finally, it should be noted that for some inversion problems, it would be more rigorous to incorporate a stochastic model that accounts for temporal correlations in the position time series. There have been several attempts to infer the stochastic nature of errors in the time domain from spectral analysis (Mao et al., 1999; Williams, 2003). The consensus conclusion of such investigations is that GPS time series has the characteristics of flicker noise. The presence of random walk noise, which is quite damaging to the determination of station velocity, for example, is much less conclusive. The importance of these models has proven to lie largely in the realistic assignment of error bars on the estimated geophysical parameters and not so much on the actual estimates themselves. Ultimately, the accuracy of geophysical parameter estimates is better inferred by other external means, such as the smoothness of the inverted velocity field in regions where smoothness is expected from geologic considerations.

As a general rule, estimation of station velocity can be achieved with precision $< 1 \text{ mm year}^{-1}$ using > 2.5 years of continuous data. One measure of precision is to infer it from the smoothness of a velocity field across a network (Davis et al., 2003). In some sense, this approach gives a measure of 'accuracy,' because the results are being compared with an assumed truth (the smoothness of the velocity field). Another method, which assesses the level of systematic error, is to compare results using different software packages. For example, Hill and Blewitt (2006) compared velocities produced using the GAMIT and GIPSY software packages, where GAMIT processes double-difference data and GIPSY processes undifferenced data. Using 4 years of data from a 30-station regional GPS network, they found that the RMS difference in GPS horizontal velocity is $< 0.1 \text{ mm year}$ (after accounting for a 14-parameter reference frame transformation between the two solutions). The data processing by both packages was done in a black-box fashion, with minimal user intervention. This result indicates that errors in GPS station velocities are more than likely to be dominated by biases in common to both GIPSY and GAMIT, for example, multipath error, antenna phase center mismodeling, and nonsecular Earth deformations.

3.11.3.3 Plate Tectonic Rotations

Once geodetic station velocities have been estimated (as outlined earlier), plate tectonic rotations can be estimated using the following classical kinematic model (Larson et al., 1997):

$$\dot{\mathbf{x}}_j^p = \boldsymbol{\Omega}^p \times \mathbf{x}_j \quad [18]$$

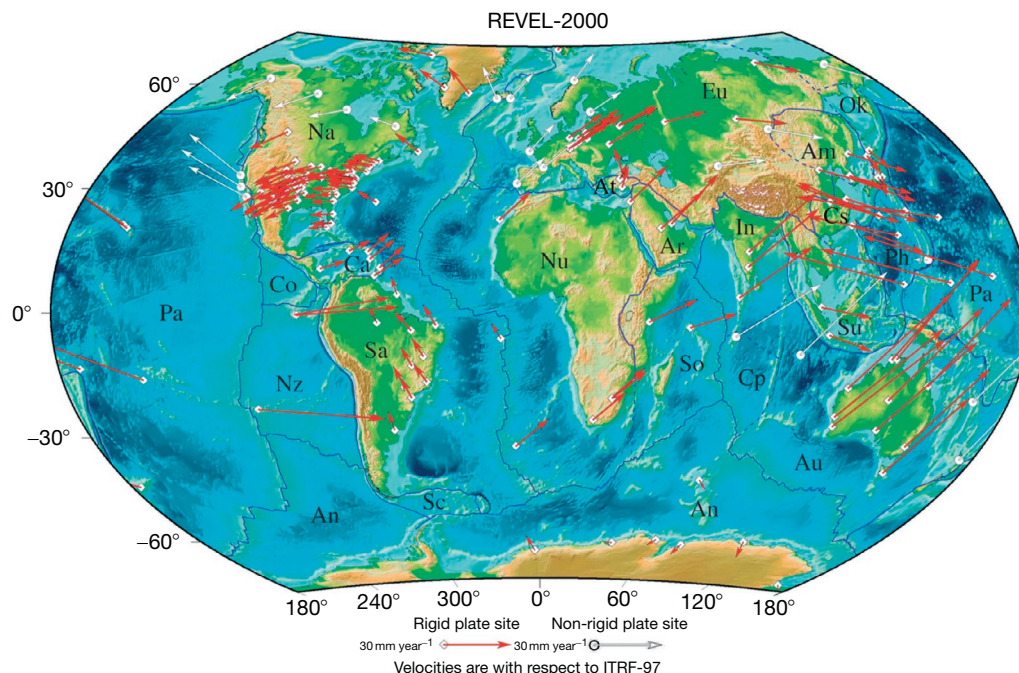
where $\boldsymbol{\Omega}^p$ is the angular velocity (sometimes called the 'Euler vector') of a plate called 'p' associated with station j. The

magnitude $\Omega^p = |\boldsymbol{\Omega}^p|$ is the 'rate of rotation' of plate p (often expressed as degrees per million years but computationally as radians per year), and the direction $\hat{\boldsymbol{\Omega}}^p = \boldsymbol{\Omega}^p / \Omega^p$ is called the 'Euler pole' (often expressed as a spherical latitude and longitude but computationally as Cartesian components, i.e., direction cosines) (Minster and Jordan, 1978). The Euler pole can be visualized as the fixed point on the Earth's surface (not generally within the plate itself) about which the plate rotates. This rotation model essentially constrains the plate to move rigidly on the Earth's surface (no radial motion). The cross product is taken between the angular velocity and station position in a geocentric reference frame; therefore, the velocity is also expressed in the geocentric reference frame. The label p on $\dot{\mathbf{x}}_j^p$ simply identifies the assumed plate (not the reference frame). This notation becomes useful later when considering the relative motion at a plate boundary.

Figure 9 shows an example of an inversion of GPS velocities for rigid plate rotations from the REVEL model (Sella et al., 2002). In this figure, only the stations so indicated were used to invert for plate rotations, on the assumption that they are located on stable plate interiors. Stations that fall within deforming plate boundaries must be treated differently, as will be explained in the following subsection.

Several points are worth noting about the classical kinematic model of plate tectonics:

- The motions are instantaneous, in the sense that the time of observation is sufficiently short that the angular velocities are assumed to be constant in time. As the equation apparently works well for paleomagnetic data over a few million



Sella, Dixon, and Mao J. Geophys. Res., 107, 10.1029/2000JB000033, 2002

Figure 9 The REVEL-2000 plate motion model derived from GPS velocities. Reproduced from Sella G, Dixon T, and Mao A (2002) REVEL: A model for recent plate velocities from space geodesy. *Journal of Geophysical Research* 107(B4), <http://dx.doi.org/10.1029/2000JB000033>.

years (DeMets et al., 1990, 1994; Minster and Jordan, 1978), such an assumption is essentially perfect for geodetic observation periods of decades. Indeed, discrepancies between angular velocities from geodesy and paleomagnetic inversions can test whether plates might have significant angular accelerations.

- Plate tectonic theory here assumes that plate motions are rigid and that the motion is a rotation about a fixed point in common to all the Earth's surface. Thus, the motions are purely horizontal on a spherical Earth.
- The assumption of plate rigidity can be tested independently of the previously mentioned model, for example, by observing changes of distance between stations supposedly on the same plate. Thus, by using geodesy (together with independent evidence), the 'stable plate interior' can be defined empirically as the domain within a plate that, to within the errors of observations, is consistent with having zero deformation. The earlier equation is therefore more properly applied to such defined 'stable plate interiors.' The relative motions between neighboring plate interiors therefore impose boundary conditions on the deformational processes that are taking place in the plate boundary region (Stein, 1993).
- Since the Earth is only approximately spherical, the earlier equation gives long systematic errors at the level of $\sim 0.2 \text{ mm year}^{-1}$, including in the vertical direction (with respect to the WGS 84 reference ellipsoid). Because the errors have a very long wavelength, the induced artificial strain rates are negligible ($< 0.1 \text{ nstrain year}^{-1}$).
- Even though vertical motions are predicted to be zero in the model, it is convenient to invert the earlier equation using Cartesian coordinates and using the full weight matrix (inverse covariance) associated with the Cartesian components of velocity. In any case, the resulting estimate of angular velocity will not be sensitive to errors in vertical velocity.
- If the true plate motions (for the part of plates exposed on the Earth's surface) are on average gravitationally horizontal (with respect to the geoid), then on average, the motion must also be horizontal with respect to the reference ellipsoid (which is defined to align with the geoid on average). Such a reference ellipsoid is necessarily centered on the center of mass of the entire Earth system, CM. Therefore, the fixed point of rotation can be taken to be CM, which is the ideal origin of ITRF. Due to the (verifiable) assumption that plate motions are constant, it is therefore important to use the long-term average CM rather than the instantaneous CM, which can move by millimeters relative to the mean Earth's surface (CF) over tidal and seasonal timescales (caused by redistribution of fluid mass).
- Any systematic error in the realization of CM will map into errors in the model for plate motions and hence errors in estimates of plate angular velocities. Significantly, this will also affect model predictions of the relative velocities of stations across plate boundaries. Considering the velocity of station j , which resides nominally on plate p (e.g., Pacific), in a reference frame corotating with plate n (e.g., North America), then this can be expressed as the following relative velocity:

$$\begin{aligned}\dot{\mathbf{x}}_j^p &= \mathbf{\Omega}^p \times \mathbf{x}_j \\ \dot{\mathbf{x}}_j^p - \dot{\mathbf{x}}_j^n &= \mathbf{\Omega}^p \times \mathbf{x}_j - \mathbf{\Omega}^n \times \mathbf{x}_j \\ \Delta \dot{\mathbf{x}}_j^{pn} &= \Delta \mathbf{\Omega}^{pn} \times \mathbf{x}_j\end{aligned}\quad [19]$$

- Here, $\Delta \mathbf{\Omega}^{pn}$ is the relative angular velocity between plates p and n , and $\Delta \dot{\mathbf{x}}_j^{pn}$ is the relative velocity between plates p and n at station j , in other words, the relative velocity of station j on plate p as viewed by an observer fixed to plate n . Note that if station j actually lies in the stable interior of plate p , then $\Delta \dot{\mathbf{x}}_j^{pn}$ represents the path integral of deformation plus rotation crossing the entire plate boundary going from the stable interior of plate n to station j . Hence, systematic errors in $\Delta \mathbf{\Omega}^{pn}$ will negatively impact geophysical inferences on plate boundary deformation. This proves that it is important to plate tectonic applications of geodesy to realize the origin of the reference frame as the long-term center of mass of the entire Earth system. Thus, from a physical standpoint, the SLR technique is essential (to realize the origin), even if it is not the primary tool for observing relative motions between plates. It is possible to realize an appropriate origin geometrically, by assuming that, after accounting for known geophysical processes that cause vertical motion (e.g., glacial isostatic adjustment), there should be no residual vertical motion in some average sense. There are various possible ways to define such an origin, and it remains a promising topic of research to understand which types of global reference frames (in terms of their realization of the velocity reference at the origin) are most appropriate for determining plate angular velocities.
- The angular velocity parameters for any given plate are going to be best constrained by a network that maximally spans the rigid plate interior. This presents a problem if the plate is small. For very small plates (e.g., blocks in plate boundary zones), the motion can be characterized by a horizontal translation to within the sensitivity of geodetic measurements. In this case, there is a high correlation between the rate of rotation and the location of the Euler pole normal to the direction plate motion, and so the concepts of rate of rotation and Euler pole essentially lose their meaning. Nevertheless, what is important to geophysical processes is not the precision of the Euler pole and rate of rotation, but rather the precision to which relative motion is known across plate boundaries. Generally, this will be constrained very well if the geodetic network spans those boundaries.

3.11.3.4 Plate Boundary Strain Accumulation

Approximately 85% of the Earth's surface can be characterized by rigid plate tectonics. The remaining 15% can be characterized as plate boundary zones, within which the Earth's crust deforms to accommodate the relative rotation between neighboring plates (Holt et al., 2005). As these zones are responsible for generating destructive earthquakes, they are the subject of intense geodetic research. To accommodate crustal deformation, the model for rigid plate rotations can be modified to a continuum velocity field $\dot{\mathbf{x}}(\mathbf{x})$ as follows:

$$\dot{\mathbf{x}}(\mathbf{x}) = \mathbf{\Omega}(\mathbf{x}) \times \mathbf{x} \quad [20]$$

where $\dot{\mathbf{x}}(\mathbf{x})$ has been parameterized in terms of a continuum angular velocity field $\mathbf{\Omega}(\mathbf{x})$, otherwise known as the 'rotational

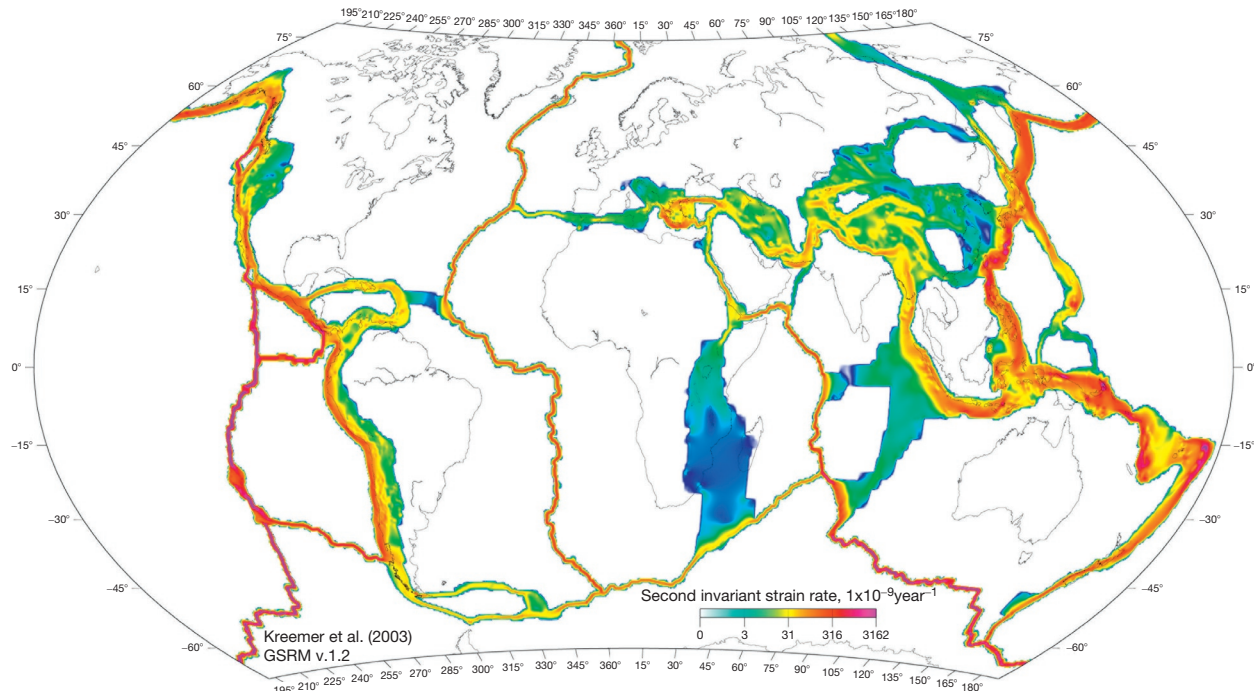


Figure 10 A global strain-rate map, derived from space geodetic data. Adapted from Kreemer C, Holt WE, and Haines AJ (2003). An integrated global model of present-day plate motions and plate boundary deformation. *Geophysical Journal International* **154**, 8–34.

vector function' (Haines and Holt, 1993). The advantage of this reparameterization is that the angular velocity field is a constant within a stable plate interior, unlike the velocity field, which appears as a rotation, depending on the defined reference frame. If a region can be defined a priori as being on a stable plate interior, then $\mathbf{\Omega}(\mathbf{x})$ can be constrained as a constant parameter in the model: $\mathbf{\Omega}(\mathbf{x}) = \mathbf{\Omega}^p$, and in these regions, the formula reduces to the plate rotation model. Otherwise, spatial gradients of $\mathbf{\Omega}(\mathbf{x})$ correspond to deformation rates. Specifically, the three horizontal components of the deformational (symmetrical and nonrotating) strain-rate tensor on a sphere can be written as

$$\begin{aligned} \dot{\epsilon}_{\varphi\varphi} &= \frac{\hat{\Theta}}{\cos\theta} \cdot \frac{\partial\mathbf{\Omega}}{\partial\varphi} \\ \dot{\epsilon}_{\theta\theta} &= -\hat{\Phi} \cdot \frac{\partial\mathbf{\Omega}}{\partial\theta} \\ \dot{\epsilon}_{\varphi\theta} &= \frac{1}{2} \left(\hat{\Theta} \cdot \frac{\partial\mathbf{\Omega}}{\partial\theta} - \frac{\hat{\Phi}}{\cos\theta} \cdot \frac{\partial\mathbf{\Omega}}{\partial\varphi} \right) \end{aligned} \quad [21]$$

where $\hat{\Theta}$ and $\hat{\Phi}$ are unit vectors that point in the north and east directions, respectively. The contribution of vertical velocity to horizontal strain rates is neglected, because this is $< 2\%$ for even rapid uplift rates of 10 mm year^{-1} . Similarly, the vertical component of the rotation rate (the symmetrical strain-rate tensor component) is

$$w = \frac{1}{2} \left(\hat{\Theta} \cdot \frac{\partial\mathbf{\Omega}}{\partial\theta} + \frac{\hat{\Phi}}{\cos\theta} \cdot \frac{\partial\mathbf{\Omega}}{\partial\varphi} \right) \quad [22]$$

The Global Strain Rate Map (GSRM) Project has implemented this approach to invert GPS station velocities for a global map of

strain (Holt et al., 2005; Kreemer et al., 2000, 2003). The GSRM website (<http://www.world-strain-map.org>) is housed and maintained at UNAVCO facility in Boulder, Colorado. The GSRM website has an introduction page where one can access information on the methodology used, the data and references, model results, and acknowledgments. A sample of a global strain-rate map is presented in Figure 10. Areas with no color (white) are constrained a priori to be stable (zero strain, corresponding to rigid plate rotation, as in the classical plate tectonic model).

Haines (1982) showed that if the spatial distribution of strain rates is everywhere defined, then the full velocity gradient tensor is uniquely defined. Given that geodetic stations only sample the continuum velocity field at a discrete set of locations, additional constraints are required to invert the equations. In early work, the rotation vector function was expanded as polynomials (Holt and Haines, 1993; Holt et al., 1991; Jackson et al., 1992), but in all later work, the bicubic Bessel interpolation on a curvilinear grid has been used for the Aegean Sea (Jackson et al., 1994), Asia (Holt et al., 1995), Iran (Jackson et al., 1995), Japan (Shen-Tu et al., 1995), the Indian Ocean (Tinnon et al., 1995), the western United States (Shen-Tu et al., 1999), New Zealand (Holt and Haines, 1995), and the Tonga subduction zone (Holt, 1995).

The art of designing appropriate constraint methods is a fertile area of research. In general, the constraints should be data-driven where there are data but should be averse to generating artifacts in sparsely sampled regions. Ideally, the constraints should adapt the spatial resolution to the extreme nonhomogeneity that is the case for today's global network of continuous GPS stations. However, it should be kept in mind that no matter what the constraints, they will generally smooth the observed velocity field to some extent and will

generally generate anomalous spatially distributed artifacts around stations with velocity errors. Such is the nature of underdetermined inversion problems. The key to successful geophysical interpretation is to not overanalyze the results and to use only information at wavelengths longer than a spatial resolution appropriate to the expected errors. One exception to this is the case where anomalous motion of a station is truly geophysical and related to an interesting localized process. Strain-rate mapping can be used to help identify such candidates for further investigation.

One method of imposing constraints is using independent strain-rate inferences from earthquake moment tensors and geologic fault slip data, through Kostrov's relation (Kostrov, 1974). Observed average seismic strain rates for any grid area can be obtained by summing moment tensors in the volume described by the product of the grid area and the assumed seismogenic thickness:

$$\dot{\epsilon}_{ij} = \frac{1}{2\mu VT} \sum_{k=1}^N M_0 m_{ij} \quad [23]$$

where N is the number of events in the grid area, μ is the shear modulus, V the cell volume, T is the time period of the earthquake record, M_0 is the seismic moment, and m_{ij} is the unit moment tensor. Similarly, average horizontal strain-rate components from Quaternary fault slip data can be obtained by a variant of Kostrov's summation (Kostrov, 1974) over N fault segments k within a grid area A :

$$\dot{\epsilon}_{ij} = \frac{1}{2} \sum_{k=1}^N \frac{L_k \dot{u}_k}{A \sin \delta_k} m_{ij}^k \quad [24]$$

where m_{ij}^k is the unit moment tensor defined by the fault orientation and unit slip vector and the fault segment has length L_k , dip angle δ_k , and slip rate \dot{u}_k .

In this combined (geodetic + seismic + geologic) scheme, an objective minimization function can then be defined that accommodates all three data types (e.g., Kreemer et al., 2000). Typically, geodetic data are given a strong weight in such schemes because, unlike the case for geodetic data, it is not clear to what extent a limited sample of earthquake moment tensors or Quaternary geologic data represent strain rates today. Whereas this approach can be applied to produce a combined (geodetic plus seismic) solution for strain-rate mapping, an alternative approach is to produce an independent empirical geodetic solution from which to compare other geophysical data types.

A different approach to strain mapping is based on the concept of 2-D tomography. The idea is that the relative velocity between distant geodetic stations must equal the path integral of strain no matter what the path. Therefore, faults can be assigned slip rates and block domains can be assigned rotations such that path integrals that cross these structures agree with the geodetic data. This approach requires the user to construct a variety of path integrals that will ensure a well-conditioned solution. Although this introduces an additional level of nonuniqueness (due to the user's choices of path integral), the resulting strain-rate maps are insensitive to the choices made so long as their choice overdetermines the problem. Implicitly, the rotation function approach also ensures that the path integral agrees in a least-squares sense with

relative velocities between stations, and so both methods lead to similar solutions, assuming the a priori constraints (from nongeodetic evidence) are approximately equivalent.

The applications of strain-rate mapping in plate boundary zones are numerous, ranging from understanding mantle-scale processes to identifying areas of enhanced seismic hazard. The general pattern of the style of strain can point to the larger-scale picture of the driving dynamics. Deformations can be understood as the sum of dilatational strain (increase in surface area) and shear strain (distortion of shape). Regions of strain that are predominantly represented by shear relate to strike-slip faulting, which typically accommodates strain across transform boundaries, such as the North America–Pacific plate boundary. Positive dilatational strain is associated with zones of extension, which can be driven by a combination of gravitational collapse and boundary conditions on a region, as is the case of the Great Basin in western North America. Gravitational collapse is a predominant factor in the Himalayas and the broader zone of deformation in Southeast Asia. Negative dilatational strain is of course associated with convergent plate boundaries. Whereas these examples are largely related to mantle-scale processes, on the smaller-scale, combinations of all styles of strains can arise from inhomogeneities in the crust. For example, kinks in a strike-slip fault can create either a compressional fold or pull-apart basins.

Clearly, all these processes can be and have been studied with nongeodetic techniques and geodesy should be considered as just one tool that can be brought to bear. Broadly speaking, what geodesy brings to the table are the following two basic advantages:

- Geodesy can provide a seamless, consistent map of strain rates spanning a broad range of distance scales, ranging from seismogenic thickness (~ 15 km) to the global scale ($\sim 10,000$ km). As such,
 - geodesy can provide a spatial framework within which other types of geophysical evidence can be better interpreted,
 - geodesy can indicate to what extent strain can be attributed to broader mantle-scale processes versus more localized crustal-scale structures,
 - a geodetic map of strain rate can provide boundary conditions for a study area within which more detailed fieldwork can be preformed and understood in the broader context.
- Geodesy can provide a seamless, consistent characterization of changes in strain- rates over the timescales of seconds to decades. As such,
 - geodesy clearly represents what is happening today (differences with other techniques may point to temporal evolution in recent geologic time),
 - geodesy is an appropriate tool to study all phases of the earthquake cycle (the topic of the next section), ranging from coseismic rupture, through postseismic relaxation, to steady-state interseismic strain accumulation.

3.11.3.5 The Earthquake Cycle

As pointed out in the previous section, geodesy can be used to investigate motions of the Earth's surface on timescales of

seconds to decades and so is an appropriate tool to study all phases of the earthquake cycle (Hammond, 2005).

Figure 11 schematically illustrates the expected characteristics of geodetic position time series as a function of time and distance from a fault through the earthquake cycle. In this specific example, the fault is strike-slip with two stations on either side of the fault located at equal distance normal to the fault strike (Figure 12). 'Displacement' is defined as the relative position of the two stations in the direction parallel to the strike of the fault. Each curve represents a different distance

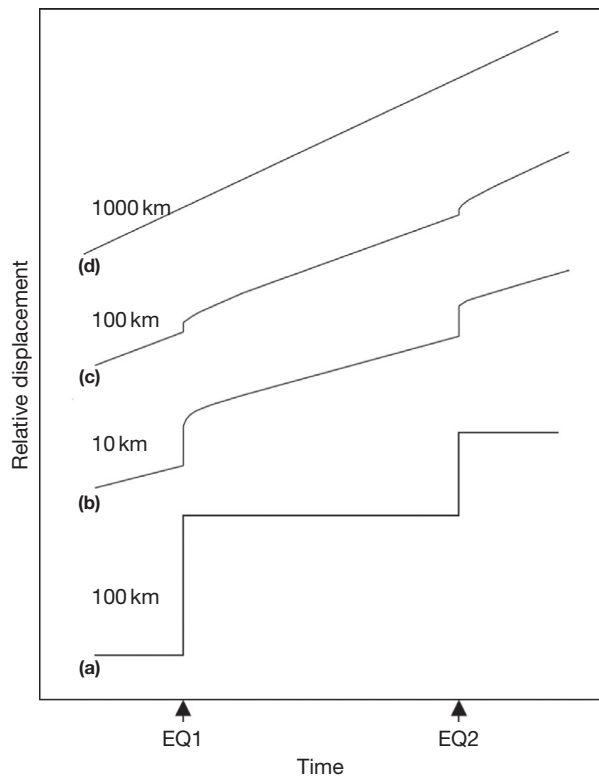


Figure 11 Schematic illustration of the effect of the earthquake cycle on geodetic station positions (see text for explanation).

from the fault (i.e., half the distance between stations). For purposes of illustration, the plot is not to scale. The plot shows the time of characteristic earthquakes EQ1 and EQ2, which are of the largest magnitude that can typically occur on this particular fault, such that smaller earthquakes produce displacements so small that they can be neglected for purposes of illustrating the earthquake cycle. Thus, EQ1 and EQ2 represent the start and end of an earthquake cycle. The size of these earthquakes ($M_w \sim 7$) is sufficient that they rupture from seismogenic depth through to the surface, with coseismic slip approximately constant with depth.

Case (a) at distance 100 m shows a displacement equal to the coseismic slip on the rupture plane. In between earthquakes, the distance between stations is so small that no deformation is detected. Hence, case (a) is effectively equivalent to a geologic determination of coseismic fault slip. In the opposite extreme, case (d) at 1000 km from the fault in the far field shows no detectable coseismic displacement. (This assumes naively that this is only active fault in the region of this scale.) This displacement represents the far-field driving force transmitted through the crust that ultimately causes the earthquakes. In a sense, the earthquake represents the crust 'catching up' to where it would be if the fault were continuously sliding as a frictionless plane. Thus, case (d) shows the same average displacement per year as would a regression to curve (a) over a sufficient number of earthquake cycles. Thus, case (d) also represents (1) the slip rate at depth below the locked (seismogenic) portion of the crust, assuming the crust behaves perfectly elastically, and (2) the mean slip rate inferred by geologic observations of recent Quaternary earthquakes over several earthquake cycles, assuming that the activity of this fault is in steady-state equilibrium and is not evolving in time.

Case (b) represents the strain accumulation and release where strain rates are highest in the near field of the fault. In this case, the coseismic displacement is slightly damped due to the coseismic rupture being of finite depth. On the other hand, the time series captures subsequent near-field postseismic effects following each earthquake (Pollitz, 1997, 2003). These processes include afterslip (creep) caused by a velocity-hardening rheology and poroelastic relaxation in response to coseismic change in pore pressure. Significant aftershock might

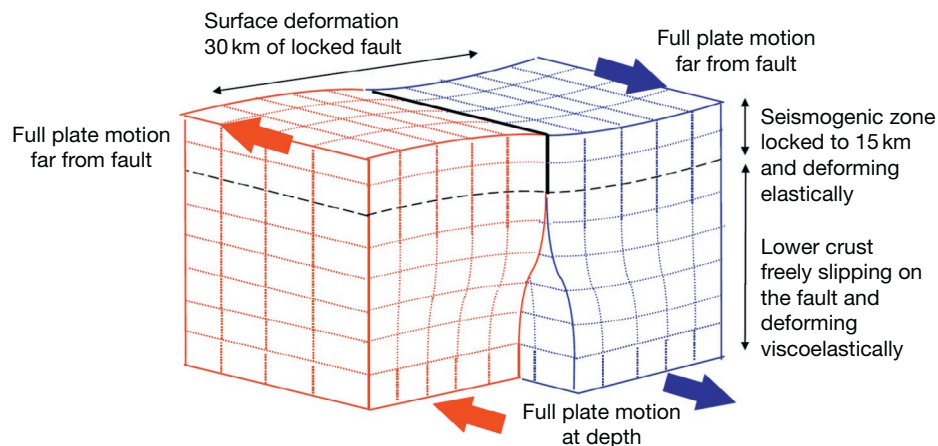


Figure 12 Deformation around a transform plate boundary, such as the San Andreas Fault.

in some cases be a contributing factor. These processes affect GPS position time series in the days to months following the earthquake (Kreemer et al., 2006a).

Over periods of years to decades, the strain for case (b) is slowly released in the viscoelastic layers beneath the crust, which will affect the time series. This occurs because at the time of the earthquake, the crust displaces everywhere and stresses the layers beneath. These layers react instantly as an elastic medium, but as time increases, they start to flow viscously. As the time series ages toward the second earthquake EQ2, most of the viscoelastic response has decayed, and the time series becomes flat. This represents the phase of interseismic strain accumulation. However, the slope of this part of the curve is significantly lessened owing to transient postseismic processes earlier in the earthquake cycle. Thus, near-field measurements of strain alone can significantly underestimate the seismic hazard unless this is taken into account. This dampening phenomenon also makes it more difficult to pinpoint the location of active faults capable of generating large earthquakes.

Stations in case (c) are still sufficiently close that coseismic displacements can be detected but are far enough from the rupture that near-field relaxation does not contribute to the time series. On the other hand, the crust in this intermediate field responds significantly to deep viscoelastic relaxation at the base of the crust and beyond, into the upper mantle. Precisely how the pattern of deformations looks in the years after a large earthquake depends on the relative effective viscosity of these various layers (Hetland and Hager, 2006). Thus, GPS networks with stations at various distances about a recently ruptured fault can be used to probe rheology versus depth. Note that in going from EQ1 to EQ2, the relative velocity between the pair of stations decreases in time. Thus, the strain rate can depend considerably on the phase of the earthquake cycle (Dixon et al., 2003). Thus, in regions of low strain where there are many faults that rupture infrequently (such as the Great Basin, western United States), it is not uncommon to observe strain rates that are almost entirely transient in nature and can exceed interseismic strain by an order of magnitude (Gourmelen and Amelung, 2005; Hetland and Hager, 2003). This makes it more difficult to interpret strain-rate maps in terms of seismic hazard, except in those cases where the strain rates are so large that logically, they must be dominated by interseismic strain accumulation on dominant faults (Kreemer et al., 2006b). Such analysis is on the leading edge of research and requires careful modeling of the earthquake cycle in any given region of interest.

3.11.3.6 Surface Mass Loading

The Earth's time-variable geometric shape, gravitational field, and rotation in space are all connected by the Earth's dynamic response to the redistribution of near-surface mass, including mass in the ocean, continental water, ice sheets, and atmosphere. As a consequence, measurements of the Earth's geometric shape from GPS can be used to infer surface mass redistribution and therefore predict changes to the gravitational field and the Earth's rotation. Thus, GPS measurements of the Earth's shape can be independently checked by comparison with time-variable gravity as measured in space by geodetic satellites or residual measurements of the Earth's rotation

(i.e., change in the Earth's rotation driven by change in moment of inertia).

Surface loading therefore represents a unifying theme in geodesy, connecting various types of geodetic measurement and geodynamic models (Figure 8). With an assumed structure and rheology of the Earth, it becomes possible to estimate surface mass redistribution from the changing shape of the Earth (Plag et al., 1996). Conversely, with a known source of mass redistribution (e.g., inferred by gravity measurements), it should be possible to invert the measured shape of the Earth to solve for the Earth's structure (and rheology, if we include the time-variable response). That is, the ratio of the Earth's gravitational response to geometric response can be used to infer the Earth's structure and rheology.

Loading models have traditionally used Green's functions, as derived by Farrell (1972) and applied in various geodetic investigations (e.g., Van Dam et al., 1994). Green's function approach is fundamentally based on load Love number theory, in which the Earth's deformation response is a function of the spherical harmonic components of the incremental gravitational potential created by the surface load. To study the interaction between loading dynamics and the terrestrial reference frame, it is convenient to use the spherical harmonic approach (Grafarend et al., 1997; Lambeck, 1988; Mitrovica et al., 1994) (therefore, the conclusions must also apply to the use of Green's functions).

The following 'standard model' is based on a spherically symmetrical, radially layered, elastic Earth statically loaded by a thin shell on the Earth's surface. Farrell (1972) used such a model to derive Green's functions that are now prevalent in atmospheric and hydrologic loading models (van Dam et al., 2001). The preliminary reference Earth model PREM (Dziewonski and Anderson, 1981) yields load Love numbers almost identical to Farrell's (Grafarend et al., 1997; Lambeck, 1988).

It is analytically convenient to decompose the Earth system as a spherical solid Earth of radius R_E , plus surface mass that is free to redistribute in a thin surface layer ($\ll R_E$) of surface density $\sigma(\Omega)$, which is a function of geographic position Ω (latitude φ and longitude λ). Let us express the total redistributed load as a spherical harmonic expansion:

$$\sigma(\Omega) = \sum_{n=1}^{\infty} \sum_{m=0}^n \sum_{\Phi=C}^S \sigma_{nm}^{\Phi} Y_{nm}^{\Phi}(\Omega) \quad [25]$$

where $Y_{nm}^{\Phi}(\Omega)$ are defined in terms of associated Legendre polynomials: $Y_{nm}^C = P_{nm}(\sin \phi) \cos m\lambda$ and $Y_{nm}^S = P_{nm}(\sin \phi) \sin m\lambda$.

The summation begins at degree $n=1$ assuming that mass is conserved in the Earth system. It is this initial degree-one term that relates to the origin of the reference frame. It can be shown (Bomford, 1971) that, for a rigid Earth, such a thin-shell model produces the following incremental gravitational potential at the Earth's surface, which we call the 'load potential':

$$V(\Omega) = \sum_n V_n(\Omega) = -\frac{4\pi R_E^3 g}{M_E} \sum_n \sum_m \sum_{\Phi} \frac{\sigma_{nm}^{\Phi} Y_{nm}^{\Phi}(\Omega)}{(2n+1)} \quad [26]$$

where g is acceleration due to gravity at the Earth's surface and M_E is the mass of the Earth. This load potential results in a

displacement of the geoid called the 'equilibrium tide.' As shall be addressed later, the load deforms the solid Earth and, in doing so, creates an additional potential.

According to load Love number theory, solutions for surface displacements $\Delta s_h(\Omega)$ in the local height direction and $\Delta s_l(\Omega)$ in any lateral direction specified by unit vector $\hat{\mathbf{l}}(\Omega)$ are given by (Lambeck, 1988)

$$\begin{aligned}\Delta s_h(\Omega) &= \sum_n h'_n V_n(\Omega)/g \\ \Delta s_l(\Omega) &= \sum_n l'_n \hat{\mathbf{l}}(\Omega) \cdot \nabla V_n(\Omega)/g\end{aligned}\quad [27]$$

and the additional potential caused by the resulting deformation is

$$\Delta V(\Omega) = \sum_n k'_n V_n(\Omega) \quad [28]$$

where h'_n , l'_n , and k'_n are degree- n load Love numbers, with the prime distinguishing Love numbers used in loading theory from those used in tidal theory. The surface gradient operator is defined as $\nabla = \hat{\boldsymbol{\phi}} \partial_\varphi + \hat{\boldsymbol{\lambda}} (1/\cos\varphi) \partial_\lambda$, where $\hat{\boldsymbol{\phi}}$ and $\hat{\boldsymbol{\lambda}}$ are unit vectors pointing northward and eastward, respectively.

The net loading potential (load plus additional potential) relative to Eulerian observer (the 'space potential' as observed on a geocentric reference surface) is

$$\begin{aligned}U(\Omega) &= V(\Omega) + \Delta V(\Omega) \\ &= \sum_n (1 + k'_n) V_n(\Omega)\end{aligned}\quad [29]$$

The net loading potential relative to Lagrangian observer (the 'body potential' as observed on the deforming Earth's surface) must also account for the lowering of the Earth's surface due to loading. From eqns [5] and [3], the body potential is

$$\begin{aligned}U'(\Omega) &= U(\Omega) - g \Delta s_h(\Omega) \\ &= \sum_n (1 + k'_n - h'_n) V_n(\Omega)\end{aligned}\quad [30]$$

Therefore, the 'space' and 'body' combinations of load Love number, $(1 + k'_n)$ and $(1 + k'_n - h'_n)$, are relevant to computing gravity acting on Earth-orbiting satellites and Earth-fixed instruments, respectively.

Solutions for surface deformations of the thin-shell loading model are found by substituting [2] into [3] and [5]:

$$\begin{aligned}\Delta s_h(\Omega) &= \frac{4\pi R_E^3}{M_E} \sum_n \sum_m \sum_\phi \frac{h'_n}{2n+1} \sigma_{nm}^\phi Y_{nm}^\phi(\Omega) \\ \Delta s_l(\Omega)^l &= \frac{4\pi R_E^3}{M_E} \sum_n \sum_m \sum_\phi \frac{l'_n}{2n+1} \sigma_{nm}^\phi \hat{\mathbf{l}} \cdot \nabla Y_{nm}^\phi(\Omega) \\ U(\Omega) &= \frac{4\pi R_E^3}{M_E} \sum_n \sum_m \sum_\phi \frac{1+k'_n}{2n+1} \sigma_{nm}^\phi Y_{nm}^\phi(\Omega)\end{aligned}\quad [31]$$

Thus, GPS data on station coordinate variations around the globe can be used to invert eqn [7] for the surface mass coefficients (up to some degree and order n) and hence the surface mass field by substitution into eqn [1] (Blewitt and Clarke, 2003). Truncation of the expansion is of course necessary due to the discrete and finite coverage of GPS data, especially considering the sparsity of data in certain areas such as over the ocean. This implies that the surface mass field will be

smoothed. Nevertheless, the long-wavelength information from geodesy is in principle useful to constrain the continental-scale integral of basin-scale hydrologic models.

While it is in widespread use, the previously mentioned standard loading model might be improved by incorporating the Earth's ellipticity (Wahr, 1981), mantle heterogeneity (Dziewonski et al., 1977; Plag et al., 1996; Su et al., 1994; van Dam et al., 1994), and Maxwell rheology (Lambeck, 1988; Mitrovica et al., 1994; Peltier, 1974). There is no consensus model to replace PREM yet; however, the general approach to reference frame considerations described here would be applicable to improved models.

To date, surface mass loading has primarily been investigated by gravimetric methods (e.g., GRACE and SLR, see elsewhere in this volume), and the application of geometric measurements from GPS is still in its infancy. The most promising application of GPS in this respect is to the lower-degree harmonic components of the global surface mass field, to which satellite missions such as GRACE are least sensitive.

References

- Altamimi Z, Angermann D, Argus D, et al. (2001) The terrestrial reference frame and the dynamic Earth. *EOS. Transactions of the American Geophysical Union* 82: 273–279.
- Altamimi Z, Sillard P, and Boucher C (2002) ITRF2000: A new release of the International Terrestrial Reference Frame for Earth science application. *Journal of Geophysical Research* 107(B10): 2214. <http://dx.doi.org/10.1029/2001JB000561>.
- Argus DF, Peltier WR, and Watkins MM (1999) Glacial isostatic adjustment observed using very long baseline interferometry and satellite laser ranging geodesy. *Journal of Geophysical Research* 104(B12): 29077–29093.
- Ashby N (2004) The Sagnac effect in the Global Positioning System. In: Rizzi G and Ruggiero ML (eds.) *Relativity and Rotating Frames (Fundamental Theories of Physics)*, vol. 135, pp. 11–28. Dordrecht: Springer.
- Ashby N and Allan D (1984) Coordinate time on and near the Earth. *Physical Review Letters* 53(19): 1858.
- Bar-Sever Y (1996) A new model for GPS yaw attitude. *Journal of Geodesy* 70: 714–723.
- Bar-Sever YE, Kroger PM, and Borjesson JA (1998) Estimating horizontal gradients of tropospheric path delay with a single GPS receiver. *Journal of Geophysical Research* 103: 5019–5035.
- Bennett RA, Wernicke BP, and Davis JL (1998) Continuous GPS measurements of contemporary deformation across the northern Basin and Range province. *Geophysical Research Letters* 25: 563–566.
- Bennett RA, Wernicke BP, Niemi NA, Friedrich AM, and Davis JL (2003) Contemporary strain rates in the northern Basin and Range province from GPS data. *Tectonics* 22(2): 1008. <http://dx.doi.org/10.1029/2001TC001355>.
- Bertiger WI, Desai SD, Haines B, et al. (2010) Single receiver phase ambiguity resolution with GPS data. *Journal of Geophysical Research* 84(5): 327–337.
- Beutler G, Brockmann E, Gurtner W, Hugentobler U, Mervart L, and Rothacher M (1994) Extended orbit modeling techniques at the CODE Processing Center of the International GPS Service for Geodynamics (IGS): Theory and initial results. *Manuscripta Geodaetica* 19: 367–386.
- Beutler G, Drewes H, and Verdun A (2004) The new structure of the International Association of Geodesy (IAG) viewed from the perspective of history. *Journal of Geodesy* 77: 560–575.
- Beutler G, Gurtner W, Bauersima I, and Langley R (1985) Modeling and estimating the orbits of GPS satellites. In: *Proceedings of the 1st International Symposium on Precise Positioning with the Global Positioning System* Rockville, MD: U.S. Dept. of Commerce.
- Beutler G, Mueller II, and Neilan RE (1994) The International GPS Service for Geodynamics: Development and start of official service on January 1, 1994. *Bulletin Geodesique* 68: 39–70.
- Bevis M, Businger S, Herring TA, Rocken C, Anthes RA, and Ware RH (1992) GPS meteorology: Remote sensing of atmospheric water vapor using the Global Positioning System. *Journal of Geophysical Research* 97(D14): 15787–15801.
- Bianco G, Devoti R, Fermi M, Luceri V, Rutigliano P, and Sciarretta C (1997) Estimation of low degree geopotential coefficients using SLR data. *Planetary and Space Science* 46: 1633–1638.

- Bierman G (1977) *Factorization Methods for Discrete Sequential Estimation*. New York, NY: Academic Press.
- Bilham R (1991) Earthquakes and sea level: Space and terrestrial metrology on changing planet. *Reviews of Geophysics* 29: 1–29.
- Blewitt G (1989) Carrier phase ambiguity resolution for the Global Positioning System applied to geodetic baselines up to 2000 km. *Journal of Geophysical Research* 94(B8): 10187–10283.
- Blewitt G (1990) An automatic editing algorithm for GPS data. *Geophysical Research Letters* 17(3): 199–202.
- Blewitt G (1993) Advances in Global Positioning System technology for geodynamics investigations. In: Smith DE and Turcotte DL (eds.) *Contributions of Space Geodesy to Geodynamics: Technology*, pp. 195–213. Washington, DC: American Geophysical Union.
- Blewitt G and Clarke P (2003) Inversion of Earth's changing shape to weigh sea level in static equilibrium with surface mass redistribution. *Journal of Geophysical Research* 108(B6): 2311. <http://dx.doi.org/10.1029/2002JB002290>.
- Blewitt G, Kreemer C, Hammond WC, Plag H-P, Stein S, and Okal E (2006) Rapid determination of earthquake magnitude using GPS for tsunami warning systems. *Geophysical Research Letters* 33: L11309. <http://dx.doi.org/10.1029/2006GL026145>.
- Blewitt G and Lavallée D (2002) Effect of annual signals on geodetic velocity. *Journal of Geophysical Research* 107(B7). <http://dx.doi.org/10.1029/2001JB000570>.
- Blewitt G and Lichten SM (1992) Carrier phase ambiguity resolution up to 12000 km: Results from the GIG'91 experiment. In: Proceedings of the 6th International Symposium on Satellite Positioning, Columbus: Ohio State University.
- Bock Y, Gourevitch SA, Counselman CC, King RW, and Abbot RI (1986) Interferometric analysis of GPS phase observations. *Manuscripta Geodaetica* 11: 282–288.
- Bock Y, Nikolaidis RM, de Jonge PJ, and Bevis M (2000) Instantaneous geodetic positioning at medium distances with the Global Positioning System. *Journal of Geophysical Research* 105(B12): 28223–28253.
- Bock Y, Prawirodirdjo L, and Melbourne TI (2004) Detection of arbitrarily dynamic ground motions with a dense high-rate GPS network. *Geophysical Research Letters* 31(B10): L06604. <http://dx.doi.org/10.1029/2003GL019150>.
- Boehm J, Niell A, Tregoning P, and Schuh H (2006) Global Mapping Function (GMF): A new empirical mapping function based on numerical weather model data. *Geophysical Research Letters* 33: L07304. <http://dx.doi.org/10.1029/2005/GL02546>.
- Bomford G (1971) *Geodesy*, third rev. ed Oxford, UK: Oxford University Press. ISBN 978-0198519195.
- Bosworth JM, Coates RJ, and Fischetti TL (1993) The Development of NASA's Crustal Dynamics Project. In: Smith DE and Turcotte DL (eds.) *Contributions of Space Geodesy to Geodynamics: Technology*, pp. 1–20. Washington, DC: American Geophysical Union.
- Boucher C and Altamimi Z (1993) Development of a conventional terrestrial reference frame. In: Smith DE and Turcotte DL (eds.) *Contributions of Space Geodesy to Geodynamics: Earth Dynamics*, pp. 89–98. Washington, DC: American Geophysical Union.
- Chao BF, O'Connor WP, Chang ATC, Hall DK, and Foster JL (1987) Snow load effect on the Earth's rotation and gravitational field, 1979–1985. *Journal of Geophysical Research* 92: 9415–9422.
- Chen G and Herring TA (1997) Effects of atmospheric azimuthal asymmetry on the analysis of space geodetic data. *Journal of Geophysical Research* 102: 20489–20502.
- Chen JL, Wilson CR, Eanes RJ, and Nerem RS (1999) Geophysical interpretation of observed geocenter variations. *Journal of Geophysical Research* 104(B2): 2683–2690.
- Cheng MK and Tapley BD (1999) Seasonal variations in low degree zonal harmonics of the Earth's gravity field from satellite laser ranging observations. *Journal of Geophysical Research* 104(B2): 2667–2681, February 10.
- Cheng M and Tapley BD (2004) Variations in the Earth's oblateness during the past 28 years. *Journal of Geophysical Research* 109. <http://dx.doi.org/10.1029/2004JB003028>.
- Choi K, Bilich A, Larson K, and Axelrad P (2004) Modified sidereal filtering: Implications for high-rate GPS positioning. *Geophysical Research Letters* 31(22), L22608.
- Ciufolini I and Pavlis EC (2004) A confirmation of the general relativistic prediction of the Lense-Thirring effect. *Nature* 431: 958–960.
- Counselman CC, Hinteregger HF, and Shapiro II (1972) Astronomical applications of differential interferometry. *Science* 178: 607–608.
- Counselman CC and Shapiro II (1979) Miniature interferometer terminals for Earth surveying. *Bulletin Geodesique* 53(2): 139–163.
- Davis JL, Bennett RA, and Wernicke BP (2003) Assessment of GPS velocity accuracy for the Basin and Range Geodetic Network (BARGEN). *Geophysical Research Letters* 30(7): 1411. <http://dx.doi.org/10.1029/2003GL016961>.
- Davis JL, Elgered G, Niell AE, and Kuehn CE (1993) Ground-based measurement of gradients in the "wet" radio refractivity of air. *Radio Science* 28: 1003–1018.
- Davis JL, Herring TA, Shapiro II, Rogers AEE, and Elgered G (1985) Geodesy by radio interferometry: Effects of atmospheric modeling errors on estimates of baseline length. *Radio Science* 20: 1593–1607.
- Davis JL, Murray MH, King RW, and Bock Y (1987) Assessing the effects of atmospheric errors on estimates of relative position obtained from GPS data. *Eos, Transactions American Geophysical Union* 68(16): 286.
- Degnan JJ (1993) Millimeter accuracy satellite laser ranging: A review. In: Smith DE and Turcotte DL (eds.) *Contributions of Space Geodesy to Geodynamics: Technology (Geodynamics Series)*, vol. 25, pp. 133–162. Washington, DC: American Geophysical Union.
- DeMets C, Gordon RG, Argus DF, and Stein S (1990) Current plate motions. *Geophysical Journal International* 101: 425–478.
- DeMets C, Gordon RG, Argus DF, and Stein S (1994) Effect of recent revisions of the geomagnetic reversal time scale on estimates of current plate motions. *Geophysical Research Letters* 21: 2191–2194.
- Devoti R, Luceri V, Sciarretta C, et al. (2001) The SLR secular gravity variations and their impact on the inference of mantle rheology and lithospheric thickness. *Geophysical Research Letters* 28(5): 855–858.
- Dickey JO, Bender PL, Faller JE, et al. (1994) Lunar laser ranging: A continuing legacy of the Apollo Program. *Science* 265: 482–490. <http://dx.doi.org/10.1126/science.265.5171.482>.
- Dixon TH (1991) An introduction to the Global Positioning System and some geological applications. *Reviews of Geophysics* 29(2): 249–276.
- Dixon TH, Golombek MP, and Thornton CL (1985) Constraints on Pacific plate kinematics and dynamics with Global Positioning System measurements. *IEEE Transactions on Geoscience and Remote Sensing* GE-23(4): 491–501.
- Dixon TH, Norabuena E, and Hotaling L (2003) Paleoseismology and GPS: Earthquake cycle effects and geodetic versus geologic fault slip rates in the eastern California shear zone. *Geology* 31: 55–58.
- Dong D and Bock Y (1989) GPS network analysis with phase ambiguity resolution applied to crustal deformation studies in California. *Journal of Geophysical Research* 94(B4): 3949–3966.
- Dow JM, Gurtner W, and Schlüter W (2005a) The IGGOS viewed from the Space Geodetic Services. *Journal of Geodynamics* 40(4–5): 375–386.
- Dow JM, Neilan RE, and Gendt G (2005b) The International GPS Service (IGS): Celebrating the 10th anniversary and looking to the next decade. *Advances in Space Research* 36(3): 320–326. <http://dx.doi.org/10.1016/j.ast.2005.05.125>.
- Dunn P, Torrence M, Kolenkiewicz R, and Smith D (1999) Earth scale defined by modern satellite ranging observations. *Journal of Geophysical Research* 26(10): 1489–1492.
- Dziewonski AM and Anderson DL (1981) Preliminary reference Earth model. *Physics of the Earth and Planetary Interiors* 25: 297–356.
- Dziewonski AM, Hager BH, and O'Connell RJ (1997) Large-scale heterogeneities in the lower mantle. *Journal of Geophysical Research* 82: 239–255. <http://dx.doi.org/10.1029/JB082i002p00239>.
- Eubanks TM (1993) Variations in the orientation of the Earth. In: Smith DE and Turcotte DL (eds.) *Contributions of Space Geodesy to Geodynamics: Earth Dynamics*, pp. 1–54. Washington, DC: American Geophysical Union.
- Evans AG, Hill RW, Blewitt G, et al. (2002) The Global Positioning System geodesy odyssey, navigation. *Journal of the Institute of Navigation* 49(1): 7–34.
- Farrell WE (1972) Deformation of the Earth by surface loads. *Reviews of Geophysics* 10: 761–797.
- Fliegel HF and Gallini TE (1996) Solar force modeling of Block IIR Global Positioning System satellites. *Journal of Spacecraft and Rockets* 33(6): 863–866.
- Fliegel HF, Gallini TE, and Swift ER (1992) Global Positioning System radiation force model for geodetic applications. *Journal of Geophysical Research* 97: 559–568.
- Frey Mueller JT and Kellogg JN (1990) The extended tracking network and indications of baseline precision and accuracy in the North Andes. *Geophysical Research Letters* 17: 207–210.
- Ge M, Gendt G, Dick G, Zhang FP, and Reigber C (2005) Impact of GPS satellite antenna offsets on scale changes in global network solutions. *Geophysical Research Letters* 32(6): L06310. <http://dx.doi.org/10.1029/2004GL022224>.
- Gegout P and Cazenave A (1993) Temporal variations of the Earth gravity field for 1985–1989 derived from LAGEOS. *Geophysical Journal International* 114: 347–359.
- Gourmelen N and Amelung F (2005) Post-seismic mantle relaxation in the Central Nevada Seismic Belt. *Science* 310: 1473–1476. <http://dx.doi.org/10.1126/science.1119798>.
- Grafarend EW, Engels J, and Varga P (1997) The spacetime gravitational field of a deforming body. *Journal of Geodesy* 72: 11–30.

- Gross RS, Blewitt G, Clarke PJ, and Lavallée (2004) Degree-2 harmonics of the Earth's mass load estimated from GPS and Earth rotation data. *Geophysical Research Letters* 31: L07601. <http://dx.doi.org/10.1029/2004GL019589>.
- Gurtner W, Beutler G, Bauersima I, and Schildknecht T (1985) Evaluation of the GPS carrier difference observations: The BERNESE second generation software package. In: Goad Clyde (ed.), *1st Int. Symp. on Precise Positioning with the Global Positioning System*, Rockville, MD: U.S. Dept. of Commerce.
- Hager BH, King RW, and Murray MH (1991) Measurement of crustal deformation using the Global Positioning System. *Annual Reviews of Planetary Science* 19: 351–382.
- Haines AJ (1982) Calculating velocity fields across plate boundaries from observed shear rates. *Geophysical Journal of the Royal Astronomical Society* 68: 203–209.
- Haines AJ and Holt WE (1993) A procedure for obtaining the complete horizontal motions within zones of distributed deformation from the inversion of strain rate data. *Journal of Geophysical Research* 98: 12057–12082.
- Hammond WC (2005) The ghost of an earthquake. *Science* 310: 1440–1442.
- Heflin MB, Bertiger WI, Blewitt G, et al. (1992) Global geodesy using GPS without fiducial sites. *Geophysical Research Letters* 19: 131–134.
- Henson DJ, Collier EA, and Schneider KR (1985) Geodetic applications of the Texas Instruments TI-4100 GPS navigator. In: Goad C (ed.), *Proceedings of the 1st International Symposium on Precise Positioning with the Global Positioning System*, pp. 191–200. Rockville, MD: U.S. Dept. of Commerce.
- Herring TA, Davis JL, and Shapiro II (1990) Geodesy by radio interferometry: The application of Kalman filtering to the analysis of very long baseline interferometry data. *Journal of Geophysical Research* 95: 12561–12581.
- Herring TA and Pearlman MR (1993) Future developments and synergism of space geodetic measurement techniques. In: Smith DE and Turcotte DL (eds.) *Contributions of Space Geodesy to Geodynamics: Technology*, pp. 21–22. Washington DC: American Geophysical Union.
- Hetland EA and Hager BH (2003) Postseismic relaxation across the Central Nevada Seismic Belt. *Journal of Geophysical Research* 108: 2394. <http://dx.doi.org/10.1029/2002JB002257>.
- Hetland EA and Hager BH (2006) The effect of rheological layering on postseismic and interseismic displacements. *Geophysical Journal International* 166: 277–292.
- Hill EM and Blewitt G (2006) Testing for fault activity at Yucca Mountain, Nevada, using independent GPS results from the BARGEN network. *Geophysical Research Letters* 33: L14302. <http://dx.doi.org/10.1029/2006GL026140>.
- Holt WE (1995) Flow fields in the Tonga slab determined from the moment tensors of deep earthquakes. *Geophysical Research Letters* 22: 989–992.
- Holt WE and Haines AJ (1993) Velocity fields in deforming Asia from the inversion of earthquake-released strains. *Tectonics* 12: 1–20.
- Holt WE and Haines AJ (1995) The kinematics of northern South Island New Zealand determined from geologic strain rates. *Journal of Geophysical Research* 100: 17991–18010.
- Holt WE, Kreemer C, Haines AJ, et al. (2005) Project helps constrain continental dynamics and seismic hazards. *Eos, Transactions of the American Geophysical Union* 86: 383–387.
- Holt WE, Li M, and Haines AJ (1995) Earthquake strain rates and instantaneous relative motions within central and east Asia. *Geophysical Journal International* 122: 569–593.
- Holt WE, Ni JF, Wallace TC, and Haines AJ (1991) The active tectonics of the Eastern Himalayan Syntaxis and Surrounding Regions. *Journal of Geophysical Research* 96: 14595–14632.
- IERS (2004) McCarthy DD and Petit G (eds.), IERS Conventions 2003, IERS Technical Note 32, Frankfurt am Main: Verlag des Bundesamts für Kartographie und Geodäsie, 127 pp., paperback, ISBN 3-89888-884-3.
- Jackson J, Haines AJ, and Holt WE (1992) Determination of the complete horizontal velocity field in the deforming Aegean Sea region from the moment tensors of earthquakes. *Journal of Geophysical Research* 97: 17657–17684.
- Jackson JA, Haines AJ, and Holt WE (1994) Combined analysis of strain rate data from satellite laser ranging and seismicity in the Aegean region. *Geophysical Research Letters* 21: 2849–2852.
- Jackson JA, Haines AJ, and Holt WE (1995) The accommodation of Arabia–Eurasia plate convergence in Iran. *Journal of Geophysical Research* 100: 15205–15219.
- Kaplan GH (1981) The IAU Resolutions on Astronomical Constants, Time Scale and the Fundamental Reference Frame, U. S. Naval Observatory Circular No. 163.
- Kedar S, Hajj GA, Wilson BD, and Heflin MB (2003) The effect of the second order GPS ionospheric correction on receiver positions. *Geophysical Research Letters* 30(16): 1829. <http://dx.doi.org/10.1029/2003GL017639>.
- King RW, Abbot RI, Counselman CC, Gourevitch SA, Rosen BJ, and Bock Y (1984) Interferometric determination of GPS satellite orbits. *Eos, Transactions of American Geophysical Union* 65: 853.
- King RW and Bock Y (2005) *Documentation for the GAMIT GPS Processing Software Release 10.2*. Cambridge, MA: Mass Inst of Technol.
- Kostrov VV (1974) Seismic moment and energy of earthquakes, and seismic flow of rocks. *Izvestiya, Academy of Sciences, USSR, Physics of Solid Earth* 1: 23–44, Eng. Transl.
- Kreemer C, Blewitt G, and Hammond WC (2006) Using geodesy to explore correlations between crustal deformation characteristics and geothermal resources. *Geothermal Resources Council Transactions* 30: 441–446.
- Kreemer C, Blewitt G, and Maerten F (2006) Co- and postseismic deformation of the 28 March 2005 Nias Mw 8.7 earthquake from continuous GPS data. *Geophysical Research Letters* 33: L07307. <http://dx.doi.org/10.1029/2005GL025566>.
- Kreemer CJ, Haines WE, Holt G Blewitt, and Lavallée D (2000) On the determination of a global strain rate model. *Earth, Planets and Space* 52: 765–770.
- Kreemer C, Holt WE, and Haines AJ (2003) An integrated global model of present-day plate motions and plate boundary deformation. *Geophysical Journal International* 154: 8–34.
- Kuang D, Rim HJ, Schutz BE, and Abusali PAM (1996) Modeling GPS satellite attitude variation for precise orbit determination. *Journal of Geodesy* 70: 572–580.
- Lambeck K (1988) *Geophysical Geodesy: The Slow Deformations of the Earth*. Oxford, UK: Clarendon Press.
- Langbein JL, Wyatt F, Johnson H, Hamann D, and Zimmer P (1995) Improved stability of a deeply anchored geodetic monument for deformation monitoring. *Geophysical Research Letters* 22: 3533–3536.
- Larson KM and Agnew D (1991) Application of the Global Positioning System to crustal deformation measurement: 1. Precision and accuracy. *Journal of Geophysical Research* 96(B10): 16547–16565.
- Larson K, Bodin P, and Gomberg J (2003) Using 1 Hz GPS data to measure deformations caused by the Denali Fault Earthquake. *Science* 300: 1421–1424.
- Larson KM, Freymueller JT, and Philippsen S (1997) Global plate velocities from the Global Positioning System. *Journal of Geophysical Research* 102: 9961–9981.
- Larson KM, Webb FH, and Agnew D (1991) Application of the Global Positioning System to crustal deformation measurement: 2. The influence of errors in orbit determination networks. *Journal of Geophysical Research* 96(B10): 16567–16584.
- Leick A (2004) *GPS Satellite Surveying*, 3rd ed. Hoboken, NJ: Wiley ISBN: 978-0-471-05930-1.
- Lichten SM and Border JS (1987) Strategies for high-precision Global Positioning System orbit determination. *Journal of Geophysical Research* 92: 12751–12762.
- MacDoran PF (1979) Satellite Emission Radio Interferometric Earth Surveying, SERIES-GPS geodetic system. *Bulletin Geodesique* 53: 117–138.
- Mader GL (1999) GPS antenna calibration at the National Geodetic Survey. *GPS Solutions* 3(1): 50–58.
- Mader GL and Czopek FM (2002) The Block IIA satellite—Calibrating antenna phase centers. *GPS World* 13(5): 40–46.
- Mao A, Harrison CGA, and Dixon TH (1999) Noise in GPS coordinate time series. *Journal of Geophysical Research* 104: 2797–2816.
- McCarthy D (ed.) (1996) IERS Conventions, IERS Tech. Note 21. Paris: IERS Central Bureau, Observatory of Paris.
- McMillan DS (1995) Atmospheric gradients from very long baseline interferometry observations. *Geophysical Research Letters* 22(9): 1041–1044.
- Meehan T, Srinivasan J, Spitzmesser D, et al. (1992) The TurboRogue GPS receiver. In: *Proc. of the 6th Intl. Symp. on Satellite Positioning, Columbus, Ohio*, 1, pp. 209–218.
- Minster JB, Altamimi Z, Blewitt G, et al. (2010) *Precise Geodetic Infrastructure: National Requirements for a Shared Resource*. Washington, DC: The National Academies Press, ISBN-10:0-309-15811-7, ISBN-13: 978-0-309-15811-4, 142 pp.
- Minster JB and Jordan TH (1978) Present-day plate motions. *Journal of Geophysical Research* 83: 5331–5354.
- Mitrovica JX, Davis JL, and Shapiro II (1994) A spectral formalism for computing three-dimensional deformations due to surface loads: 1. Theory. *Journal of Geophysical Research* 99: 7057–7073.
- Moore AW (2007) The International GNSS Service: Any questions? *GPS World* 18(1): 58–64.
- Nerem RS, Chao BF, Au AY, et al. (1993) Time variations of the Earth's gravitational field from satellite laser ranging to LAGEOS. *Geophysical Research Letters* 20(7): 595–598.
- Niell A (1996) Global mapping functions for the atmospheric delay at radio wavelengths. *Journal of Geophysical Research* 101(B2): 3227–3246.
- Nikolaidis RM, Bock Y, de Jonge PJ, Agnew DC, and Van Domselaar M (2001) Seismic wave observations with the Global Positioning System. *Journal of Geophysical Research* 106(B10): 21897–21916.
- Pearlman MR, Degnan JJ, and Bosworth JM (2002) The international laser ranging service. *Advances in Space Research* 30(2): 135–143.

- Peltier WR (1974) The impulse response of a Maxwell Earth. *Reviews of Geophysics and Space Physics* 12: 649–669.
- Plag HP, Ambrosius B, Baker TF, et al. (1998) Scientific objectives of current and future WEGENER activities. *Tectonophysics* 294: 177–223.
- Plag H-P, Juttner H-U, and Rautenberg V (1996) On the possibility of global and regional inversion of exogenic deformations for mechanical properties of the Earth's interior. *Journal of Geodynamics* 21: 287–309.
- Pollitz FF (1997) Gravitational-viscoelastic postseismic relaxation on a layered spherical Earth. *Journal of Geophysical Research* 102: 17921–17941.
- Pollitz FF (2003) Post-seismic relaxation theory on a laterally heterogeneous viscoelastic model. *Geophysical Journal International* 154: 1–22.
- Prescott WH, Davis JL, and Svarc JL (1989) Global Positioning System measurements for crustal deformation: Precision and accuracy. *Science* 244: 1337–1340.
- Ray J (ed.) (1998) IERS Analysis Campaign to Investigate Motions of the Geocenter, International Earth Rotation Service Tech. Note 25, Obs. Paris.
- Rogers AEE, Knight CA, Hinteregger HF, et al. (1978) Geodesy by radio interferometry: Determination of a 1.24-km base line vector with –5-mm repeatability. *Journal of Geophysical Research* 83: 325–334.
- Rothacher M, Beutler G, Gurtner W, Schildknecht T, and Wild U (1990) *BERNESE GPS Software Version 3.2*. Switzerland: Printing Office Univ of Berne.
- Rothacher M, Springer TA, Schaer S, and Beutler G (1998) Processing Strategies for Regional Networks. In: Brunner FK (ed.) *Advances in Positioning and Reference Frames, IAG Symposium No. 118*, pp. 93–100.
- Rummel R, Rothacher M, and Beutler G (2005) Integrated Global Geodetic Observing System (IGGOS)—Science rationale. *Journal of Geodynamics* 40(4–5): 357–362.
- Sabadini R, Di Donato G, Vermeersen LLA, Devoti R, Luceri V, and Bianco G (2002) Ice mass loss in Antarctica and stiff lower mantle viscosity inferred from the long wavelength time dependent gravity field. *Geophysical Research Letters* 29(10).
- Savage JC (1983) Strain accumulation in the Western United States. *Annual Review of Earth and Planetary Sciences* 11: 11–41. <http://dx.doi.org/10.1145/annurev. ea.11.0501083.000303>.
- Schlüter W, Himwich E, Nothnagel A, Vandenberg N, and Whitney A (2002) IVS and its important role in the maintenance of the global reference systems. *Advances in Space Research* 30(2): 145–150.
- Schmid R and Rothacher M (2003) Estimation of elevation-dependent satellite antenna phase center variations of GPS satellites. *Journal of Geodesy* 77: 440–446. <http://dx.doi.org/10.1007/s00190-003-0339-0>.
- Schmid R, Rothacher M, Thaller D, and Steigenberger P (2005) Absolute phase center corrections of satellite and receiver antennas impact on GPS solutions and estimation of azimuthal phase center variations of the satellite antenna. *GPS Solutions* 9(4): 283–293.
- Schupler BR, Allshouse RL, and Clark TA (1994) Signal characteristics of GPS user antennas. *Journal of the Institute of Navigation* 41: 277–295.
- Segall P and Davis JL (1997) GPS applications for geodynamics and earthquake studies. *Annual Reviews of Earth and Planetary Sciences* 25: 301–336.
- Sella G, Dixon T, and Mao A (2002) REVEL: A model for recent plate velocities from space geodesy. *Journal of Geophysical Research* 107(B4). <http://dx.doi.org/10.1029/2000JB000033>.
- Shapiro II (1964) Fourth test of general relativity. *Physical Review Letters* 13(26): 789–791. <http://dx.doi.org/10.1103/PhysRevLett.13.789>.
- Shen-Tu B, Holt WE, and Haines AJ (1995) Intraplate deformation in the Japanese Islands: A Kinematic study of intraplate deformation at a convergent plate margin. *Journal of Geophysical Research* 100: 24275–24293.
- Shen-Tu B, Holt WE, and Haines AJ (1999) The kinematics of the western United States estimated from Quaternary rates of slip and space geodetic data. *Journal of Geophysical Research* 104: 28927–28955.
- Silver PG, Bock Y, Agnew D, et al. (1999) A plate boundary observatory. *IRIS Newsletter* 16: 3–9.
- Smith DE and Turcotte DL (eds.) (1993) *Contributions of Space Geodesy to Geodynamics: Technology*. Washington, DC: American Geophysical Union.
- Smith KD, von Seggern D, Blewitt G, et al. (2004) Evidence for deep magma injection beneath Lake Tahoe, Nevada-California. *Science* 305: 1277–1280. <http://dx.doi.org/10.1126/science.1101304>.
- Sovers OJ and Border JS (1987) *Observation Model and Parameter Partials for the JPL Geodetic Software, "GPSOMC"*. Pasadena, CA: JPL Pub Jet Propulsion Laboratory, 87–21.
- Steigenberger P, Rothacher M, Dietrich R, Fritsche M, Rülke A, and Vey S (2006) Reprocessing of a global GPS network. *Journal of Geophysical Research* 111: B05402. <http://dx.doi.org/10.1029/2005JB003747>.
- Stein S (1993) Space geodesy and plate motions. In: Smith DE and Turcotte DL (eds.) *Contributions of Space Geodesy to Geodynamics: Crustal Dynamics*, pp. 5–20. Washington, DC: American Geophysical Union.
- Su W, Woodward RL, and Dziewonski AD (1994) Degree 12 model of shear velocity heterogeneity in the mantle. *Journal of Geophysical Research* 99: 6945–6980.
- Swift ER (1985) NSW's GPS orbit/clock determination system. In: *Proc. of the 1st Symp. on Prec. Positioning with the Global Positioning System, U.S. Dept. of Commerce, Rockville, MD*.
- Tapley BD, Schutz BE, Eanes RJ, Ries JC, and Watkins MM (1993) LAGEOS laser ranging contributions to geodynamics, geodesy and orbital dynamics. In: Smith DE and Turcotte DL (eds.) *Contributions of Space Geodesy to Geodynamics: Earth Dynamics*, pp. 147–174. Washington, DC: American Geophysical Union.
- Tavernier G, Fagard H, Feissel-Vernier M, et al. (2005) The International DORIS Service, IDS. *Advances in Space Research* 36(3): 333–341.
- Thomas JB (1988) *Functional Description of Signal Processing in the Rogue GPS Receiver*. Pasadena, CA: JPL, pp 88–15.
- Tinnon M, Holt WE, and Haines AJ (1995) Velocity gradients in the northern Indian Ocean inferred from earthquake moment tensors and relative plate velocities. *Journal of Geophysical Research* 100: 24315–24329.
- Torge W (2001) *Geodesy*, 3rd ed. Berlin, Germany: Gruyete ISBN: 978-3110170726, 400 pp.
- Tralli DM, Dixon TH, and Stephens SA (1988) The effect of wet tropospheric path delays on estimation of geodetic baselines in the Gulf of California using the Global Positioning System. *Journal of Geophysical Research* 93(B6): 6545–6557.
- Tralli DM and Lichten SM (1990) Stochastic estimation of tropospheric path delays in Global Positioning System geodetic measurements. *Bulletin Geodesique* 64: 127–159.
- Tregoning P and Herring TA (2006) Impact of a priori zenith hydrostatic delay errors on GPS estimates of station heights and zenith total delays. *Geophysical Research Letters* 33: L23303. <http://dx.doi.org/10.1029/2006GL027706>.
- Truehaft RN and Lanyi GE (1987) The effects of the dynamic wet troposphere on radio interferometric measurements. *Radio Science* 22: 251–265.
- Van Dam T, Blewitt G, and Heflin MB (1994) Atmospheric pressure loading effects on GPS coordinate determinations. *Journal of Geophysical Research* 99: 23939–23950.
- Van Dam TM, Wahr J, Milly PCD, Shmakin AB, Blewitt G, and Larson KM (2001) Crustal displacements due to continental water loading. *Geophysical Research Letters* 28: 651–654.
- Wahr JM (1981) Body tides on an elliptical, rotating, elastic and oceanless Earth. *Geophysical Journal* 64: 677–703.
- Watkins MM and Eanes RJ (1997) Observations of tidally coherent diurnal and semidiurnal variations in the geocenter. *Geophysical Research Letters* 24: 2231–2234.
- Wdowinski S, Bock Y, Zhang J, Fang P, and Genrich J (1997) Southern California Permanent GPS Geodetic Array; spatial filtering of daily positions for estimating coseismic and postseismic displacements induced by the 1992 Landers earthquake. *Journal of Geophysical Research* 102(B8): 18057–18070.
- Webb FH and Zumberge JF (1993) *An Introduction to GIPSY-OASIS II*. Pasadena, CA: Jet Propulsion Laboratory, JPL Publication D-11088.
- Wernicke BP, Friedrich AM, Niemi NA, Bennett RA, and Davis JL (2000) Dynamics of plate boundary fault systems from Basin and Range Geodetic Network (BARGEN) and geologic data. *GSA Today* 10(11): 1–7.
- Williams SDP (2003) The effect of coloured noise on the uncertainties of rates estimated from geodetic time series. *Journal of Geodesy* 76: 483–494. <http://dx.doi.org/10.1007/s00190-002-0283-4>.
- Williams JG, Boggs DH, Yoder CF, Ratcliff JT, and Dickey JO (2001) Lunar rotational dissipation in solid body and molten core. *Journal of Geophysical Research* 106(E11): 27933–27968.
- Williams JG, Tunyshev S, and Boggs DH (2004) Progress in lunar laser ranging tests of relativistic gravity. *Physical Review Letters* 93. <http://dx.doi.org/10.1103/PhysRevLett.93.261101>.
- Wilson P and Reinhart E (1993) The Wegener-Medias Project preliminary results on the determination of the geokinematics of the Eastern Mediterranean. In: Smith DE and Turcotte DL (eds.) *Contributions of Space Geodesy to Geodynamics: Crustal Dynamics*, pp. 299–310. Washington, DC: American Geophysical Union.
- Wu JT, Wu SC, Hajj GA, Bertiger WI, and Lichten SM (1993) Effects of antenna orientation on GPS carrier phase. *Manuscripta Geodaetica* 18: 91–93.
- Wyatt F (1982) Displacement of surface monuments; horizontal motion. *Journal of Geophysical Research* 87: 979–989.
- Ziebart M, Cross P, and Adhya S (2002) Modeling photon pressure, the key to high-precision GPS satellite orbits. *GPS World* 13(1): 43–50.
- Zumberge JF, Heflin MB, Jefferson DC, Watkins MM, and Webb FH (1997) Precise point positioning for the efficient and robust analysis of GPS data from large networks. *Journal of Geophysical Research* 102(B3): 5005–5018.